

Investigation of Drag-Free Control Technology for Earth Science Constellation Missions

Final Study Report
15 May, 2003

Submitted to:
NASA Earth Science Technology Office

Study Lead:
Jesse Leitner, Code 591
NASA Goddard Space Flight Center
Mission Engineering and Systems Analysis Division

Team members and contributors:
Scott Starin, NASA GSFC, Code 595
Melissa Fleck, NASA GSFC, Code 595
Bo Naasz, NASA GSFC, Code 595
Robert Fall, Honeywell Space Systems, Clearwater, FL

I. Executive Summary

Drag-free control (DFC) is a concept that initiated in the late 1960's and came to fruition in the early 1970's through several flight experiments conducted by the U.S. Navy. The experiments were successful in validating the concept and the technology transitioned into the field of gravity measurement and gravity wave detection for missions such as GRACE, Microscope, and LISA. In all of these applications, the drag-free sensor acts as a precision instrument, very high in cost, which enables the negation of the effects of non-gravitational forces acting on the vehicle through simple feedback control. These forces include drag (the atmospheric force countering the velocity direction of the vehicle), solar radiation pressure, and solar winds, so the DFC expression certainly generalizes the use of the term "drag". This study investigates a potential deviation of the technology path for drag-free control, in particular one of low-precision and high production (low cost per unit). Specifically, the fundamental question was whether DFC could be applied to a constellation of spacecraft to simplify and reduce the cost of operations, as well as improve performance. In this context, it was most important to consider the DFC sensor as being positioned subserviently to the rest of the spacecraft design (i.e., the DFC sensor is not the payload or instrument and henceforth cannot necessarily be positioned at the center of gravity of the vehicle). The question of utility can be answered through a combination of system complexity, fuel consumption, cost of the components (including technology development), cost of operations, and performance improvement (in this case, reduced navigation errors).

Assumptions:

Initially, a laser altimetry mission was selected as a reference point for analysis. The mission scenarios were provided by Dr. John Ries of the Center of Space Research at the University of Texas at Austin. However, the altitudes of such a mission (examples being 500 km polar, 800 km, or 1300 km) are in the range where drag becomes less significant than other effects, particularly those due to gravity. Analyses tied to any of these point designs would have guided the effort to misleading conclusions about the applicability of DFC. Henceforth, the approach was to identify the boundaries of applicability and then see how the applications map within the boundary. Detailed spacecraft data were taken from the Global Precipitation Measurement Mission (GPM) and the Microwave Anisotropy Probe (MAP) Mission, in terms of mass properties, ballistic coefficient, and deviation of the center of gravity (cg) from original design. While wide ranges of values were used for mass, ballistic coefficient, cg offset, and other parameters, a reference point was used for nominal analysis that had the values of 2000 kg mass, ballistic coefficient of 200 kg/m^2 , worst case cg offset of 10 cm, all of which were representative of the GPM and MAP missions. Based on initial complexities in the sensor design, particularly charge buildup and general risk of collision between proof mass and its chamber, the problem was constrained to circular or nearly circular orbits only, with earth-pointing, three-axis stabilized vehicles (the concept does not apply to spinners). The attitude control system is assumed to be tolerant to attitude corrections of the vehicle without substantial added cost. Lastly, for the constellation problem, all vehicles must be placed in orbits whose differential effect is invariant to the J_2 (Earth-oblateness) perturbation. The simplest approach for this is to have them all at the same inclination.

Summary of Results from Technical Objectives

1. *Develop an optimal control correction algorithm to ensure uniform consumption of fuel over the spacecraft constellation and subsequently determine the overall fuel consumption for such an architecture.* This simple compensation scheme is described in Section V. Because there is little sensitivity to variations in the dynamics, the control system required is quite simple for the low precision requirements for this concept and linear dynamics of relative motion are always sufficient. The absolute level of fuel consumption varies significantly with altitude. **For an altitude of around 350 km, the study showed that the ΔV per spacecraft is around 6 m/sec per month for the continuously drag-compensated case** with a ballistic coefficient of 100 kg/m².
2. *Compare the fuel consumption to a traditional approach of allowing each satellite's orbit to decay for 2-4 weeks and applying a $\Delta-V$ correction.* The most significant benefit of continuous, closed-loop drag compensation is realized for low altitudes and "non-ballistic" spacecraft. From Table 3 on p. 15 in the report, for a 350 km altitude circular orbit and a non-ballistic spacecraft (ballistic coefficient of 25 kg/m²), **the continuously drag-compensated system uses less than 50% of the fuel of that corrected once after 4 weeks.** It is important to note that for the constellation problem, the spacecraft must be in J2-invariant orbits (orbits that are not subject to differential perturbations due to J2 between spacecraft). Continuous compensation of J2 effects is substantially more costly than periodic corrections. Therefore, in this study, the scope was confined only to J2-invariant orbits. A sufficient condition for this would be the reasonable assumption that all spacecraft are in the same inclination.
3. *Compare and contrast this approach for handling the 30 spacecraft control problem to traditional means based on extensions of single spacecraft control approaches.* This closed-loop approach for constellation control provides substantial simplification of operations compared to traditional approaches. However, **there is little, if any, simplification or reduction in cost for ground-operations compared to the similar approach of continuously compensating drag using closed-loop feedback of on-board Global Positioning System (GPS) measurements.** This assessment is based on discussions with GlobalStar and Iridium operations personnel. It is, however, a straightforward fact that **the local control problem (i.e., the feedback control loop) is much simpler for drag-free control as compared to the closed-loop around GPS** because no filtering is required (hence there is no susceptibility to single-event upsets or other processing problems or constraints) and because the DFC system is only correcting local small changes between spacecraft and individual proof mass (hence linearity of the spacecraft-proofmass relative motion is preserved and the dynamics are simpler).
4. *Determine a break-even point where the number in the constellation is large enough to indicate that such an option is cost effective (even if the number is determined to be 1).* It is important to note that only a qualitative assessment can be stated because the comparison can only be made to a few example cases. In comparison to traditional means for operations, **the drag-free system will begin to pay off for a system of between 3 and 5 spacecraft in a high-drag environment** with non-ballistic spacecraft.

A fair assumption would be three operators per spacecraft if they are operating as a cluster or where careful attention must be paid to their coverage or relative separations. In such a case, operations costs can total around \$7 million/year whereas the DFC system would run about \$150k for all sensors, \$450k/year for operations costs, and an estimated \$20 million total for non-recurring engineering costs (taken at the high end of the estimated cost range from the Honeywell element of this effort). **For less drag-intensive scenarios the payoff can occur at 15-20 spacecraft** as the number of operators per spacecraft and complexity of operations for the non-DFC system go down. There are two key caveats to this. First, it is important to keep in mind the need for J2 invariant orbits between spacecraft. Second, while the navigation and control system will be much simpler than that required for a system employing GPS feedback control, the overall operations cost will not likely improve substantially (if at all) with the DFC system compared to a system with closed-loop around GPS measurements, although the costs of developing a robust feedback control system will be reduced.

5. *Compare the effects of drag-based constellation decay vs. effects due to the earth-oblateness perturbation.* In fact, early in the effort (described in the first technical section), two contradictory phenomena became clear – first, that **continuous compensation of drag is much more fuel-efficient than infrequent drag-makeup** and second, that **periodic correction of J2 perturbations is more efficient than continuous**. With this contradiction and a standard desire to design formations and constellations with minimal differential force effects, it was a simple choice to **impose a design constraint that the spacecraft orbits will not be pulled apart by the J2 perturbation**. The lack of such a constraint would lead to wasteful fuel consumption and it is unlikely that any direct science requirement would conflict with such a constraint. The significant gravitational effect was due to the cg offset and this turns out to be one of the major constraints of the DFC system.

Lastly, it is important to summarize the effects of eliminating drag on navigation errors when used in conjunction with GPS and advanced GPS filters. Described in detail in Section VIII, it was determined that **a 30%-50% reduction in navigation error is achievable if drag were to be removed** from the equations of motion using an advanced, high-fidelity filter without ground augmentation. Specifically a reduction from 6 m to 3 m in real-time on-board navigation error can be achieved with the coupled GPS/DFC system.

II. Extended Summary of Observations:

The following list describes the conclusions and observations:

1. The use of continuous control for drag makeup (as would be required for a DFC system) is substantially more fuel-efficient than less-frequent periodic DV orbital corrections. Perhaps this appears to be an obvious conclusion but corrections due to J2 perturbation to the orbit are much more expensive when performed continuously as compared to infrequent periodic corrections. This leads to the requirement that a DFC system be considered only for constellations of satellites all in the same inclination, or more generally, in J2-invariant orbits.
2. For characteristic spacecraft in 2000 kg class, at altitudes below 450 km, the force required to correct the drag is less than that required to correct for the cg offset. Above 450 km, the mere employment of a DFC system doubles the amount of net perturbing acceleration which must be compensated as compared to a spacecraft not employing DFC. Based on conclusion 1, this only doubles the fuel consumption if compared to a satellite whose drag is continuously compensated throughout the orbit. If the cg offset were reduced to 1 cm, this altitude crossover only increases to about 600 km, and to 1 mm would bring it to just under 800 km. Therefore, the gravitational effects really begin to take over at an altitude of about 500 km. The effect reverses itself at extremely high altitudes (just below geosynchronous altitude), where solar radiation pressure begins to dominate over gravity. The bottom line is that for a mission higher than about 450 km, there must be substantial savings in operations cost to see a payoff for a drag-free system.
3. There is a nominal improvement of 30-50% in navigation error using GPS measurements when drag is removed from the equations of motion as is the case for the drag free system. For example the residual errors in absolute navigation are reduced from about 6 m down to 3 m assuming that the ionosphere is properly compensated, a good assumption when an advanced filter is employed such as the GPS-Enhanced On-board Navigation System (GEONS) from GSFC, or JPL's GIPSY-OASIS. The comparison is made to on-board, real-time determination accuracies, not to ground-enhanced, post-processed, differential GPS approaches, which can substantially reduce these errors in a non-real-time sense.
4. There is potential for substantial cost savings for very large constellations of spacecraft with long lifetimes if they are in a location with substantial drag effects. The determination of the payoff "knee-in-the-curve" is purely qualitative and it is based on those missions that require substantial and frequent corrections due to drag (in low altitude orbits) or solar radiation pressure (in very high altitude orbits). This can only be determined based on empirical data from the few example large constellations that exist (or existed), such as GPS, GlobalStar, and Iridium. For the case of the GPS constellation, the spacecraft are in very stable orbits, at high altitudes, and the same inclinations. Thus the corrections to orbit are due to SRP and they are performed approximately once per month. Eliminating the SRP would not substantially change the operations level of effort as most of the ground-based monitoring is for the purpose of monitoring and dealing with anomalies, with less frequent orbit corrections. The GlobalStar constellation has 48

spacecraft at 1400 km altitude with GPS on-board. GPS provides excellent time and navigation service and henceforth the operations are simple. Each spacecraft has an orbit correction (mainly due to SRP and minimal drag) about once every two months. The staff required is minimal. The Iridium Constellation does not have GPS and henceforth has a tremendous entourage required for ground support, even at the relatively high 780 km. A significant amount of this ground support is dedicated to both time corrections and orbit determination and orbit correction.

5. One of the biggest problems associated with long-term behavior of a constellation or formation is the propagation of errors in the initial conditions, in particular, the semi-major axis. The DFC constellation will still be subject to such errors and will require on-board or ground-based sensors to deal with the problem.
6. Substantial effort in optimization will be required for fuel balancing if there is significant differential drag among the spacecraft.
7. The primary competitor to this approach for autonomous control for a constellation would be a closed loop control system using GPS as a sensor. If the mission has navigation (orbit determination or position measurement) requirements, then ground tracks, GPS, or another sensing approach will be necessary in addition to the DFC sensor. However, in either case, the closed loop architecture will be much simpler for the DFC system as compared to a closed-loop GPS-based system because there is no reliance on complex filtering schemes or the availability of GPS and the feedback is based on a simple measurement (or set of measurements) internal to the system. Likewise, such a simple control system will not be sensitive to single-event upsets, latch-ups, or other processor related issues (other than a complete failure or shutdown of the control computer).
8. While the reference spacecraft given primary consideration is a rather large 2000 kg spacecraft with ballistic coefficient of 200 kg/m^2 , strong consideration was given for microspacecraft (200 kg and less) applications. Unfortunately, there is no consistent set of statistics for microspacecraft ballistic coefficients. The certainties are that (1) the values are virtually always less than the maximum coefficients for large spacecraft, (2) there is generally little variation between the maximum and minimum values for the same microspacecraft, and (3) for large spacecraft there is frequently substantial variation between the maximum and minimum values. On the one hand, for the microspacecraft problem, all of the components are packed into a much smaller volume, henceforth with smaller wetted area for a common mass. However, it is clear after participating in spacecraft design studies for microspacecraft that one of the biggest problems is a minimum requirement for exposed area for body-mounted solar arrays to generate sufficient power. With this constraint adjoined with that of a trend of reduced spacecraft component mass, we can expect much smaller ballistic coefficients for future microspacecraft. This is not, in general, a good thing, but it does give promise for the DFC application. Furthermore, we can expect significant reduction in "travel" of the center of gravity, feasibly down to one centimeter. Henceforth, given long-term

projections for microspacecraft, the domain of application can be raised as high as 700 km altitudes.

9. Viability of this approach depends on large numbers in more ways than one. In the conclusions above, it is pointed out that, operationally speaking, payoff occurs when the number of spacecraft brings operational complexity to into a substantially challenging realm. From a commercialization standpoint, this problem becomes even more extreme. Since no low-cost DFC sensor exists today, nor one designed for long-life, much technology must be developed. Without plans for development in the dozens, possibly the hundreds, the technology will not be affordable on a per-spacecraft basis.

III. Program Background, Scope, and Objectives

Typical Low Earth Orbiting (LEO) missions for the Earth Science (ES) Enterprise apply significant ground resources to orbit determination, prediction, and correction (or stationkeeping) tasks. The most uncertain part of solving the ground-based and on-board LEO orbit determination problems is the prediction of atmospheric drag levels. Moreover, atmospheric drag forces that produce orbit decay can vary significantly from day to day and this uncertainty demands increased spacecraft tracking and detailed orbit modeling, determination, and analysis to determine the vehicle positions as well as to control it with periodic propulsive maneuvers. Elimination of drag from the spacecraft flight dynamics equations of motion reduces the orbital decay problem to gravity-induced perturbations that are well known and can be compensated for with appropriate analysis.

This study has evaluated a closed-loop control system architecture concept that provides precision orbit determination/maintenance capabilities needed for future ES LEO constellation and, in some cases, formation-flying applications. This study was to evaluate whether a drag-compensation system could provide the following benefits to a LEO spacecraft constellation:

- Compensate drag effects on spacecraft to prevent orbit decay.
- Help maintain constellation elements within their “constellation or formation tolerance parameters.”
- Reduce, and in some cases eliminate, mission downtimes required to perform ground-initiated Δ -V orbit corrections.
- Reduce uncertainty from the navigation, or orbit determination, problem to allow precise position knowledge.
- Simplify station-keeping of large constellations, including limiting the amount of manpower required to control a constellation (the GPS constellation would be a good reference problem) and reduce reliance on complex collision avoidance algorithms.

Prior work in this area has centered around the single spacecraft drag-free control (DFC) problem and has involved building the spacecraft around the center, in a sense eliminating one of

the biggest system level challenges in developing such a system. Therefore, this effort had two primary unique foci: (1) start from the ground up with the fundamental affects of placement of such a sensor without confining it to the vehicle cg (henceforth, so that the approach will be applicable to general classes of missions without applying complex constraints on mass distributions which can never be met) and (2) identify the feasibility, utility, affordability, and applicability for substantially simplifying the constellation maintenance problem for medium – large constellations by employing a DFC system on each spacecraft.

Scope

There were two primary goals of this study. The first was to answer the question: *What degree of orbit precision improvement can be obtained by the application of a drag-compensation system such as the one described above, and how will this improve the performance of ES missions?* The second was to answer: *How substantially can the constellation management operational infrastructure (number of personnel required, the frequency of Δ -Vs required among the constellation, etc.) be reduced by such a system?*

To understand potential benefits of the drag-free concept this study was to:

1. Perform an assessment to determine the type/class of ES missions that would benefit the most from drag-free technology.
2. Perform trades to identify the most advantageous drag-free system architectures, define performance requirements for each architectural ‘case’, and compare the drag-free approach with alternative large-scale approaches for constellation control.
3. Evaluate the technical feasibility and cost of outfitting drag free technology to “reference spacecraft” for the mission ‘cases’ identified in (1).
4. Perform an assessment of cost/benefit ratio performance of the drag-free technology used alone vs. alternative or complementary configurations of drag compensation. For this, each of the approaches anticipated requires estimation algorithms that have unique drag-dependent terms. To do this comparison, we will use ES missions ‘cases’ (e.g. an altimetry mission, and a multi-spacecraft interferometric synthetic aperture radar (SAR) mission) and use their requirements as drivers for the analysis

Study Approach

Initially in this study, the approach was to apply DFC methodology to some selected mission concepts deemed as appropriate use cases. However, during the initial formulation of the governing equations, it became clear why the multi-spacecraft DFC problem holds some very unique issues relative to the single spacecraft version. Aside from differential drag effects which are difficult to model realistically and which can lead to non-uniform fuel consumption throughout the constellation, the differential J_2 (Earth-oblateness) effect can cause a secular

decay of the constellation which would be too fuel intensive to correct. This is not unique to a DFC-based constellation and requires that standard methods be used in the constellation design such that the relative positions of the spacecraft are not affected by J2 (aka, J2-invariant orbits). The simplest example is the case where all spacecraft are at the same inclination.

High-fidelity simulation models have been developed that incorporate vehicle dynamics including relevant perturbations, drag-free sensor dynamics and characteristics, thruster dynamics and characteristics, and other relevant quantities. Models are set up parametrically to allow technology and performance trades. Honeywell was tasked the affordability question throughout this study, based on development costs and commercialization potential. Their contribution is summarized in the Appendix.

A drag-free sensing and control architecture will be designed which is optimized for large spacecraft constellations but applicable to single spacecraft missions as well. Low-level control laws have developed based on classical control methods.

The sensing and control architecture has been integrated into the models for each of the two mission concepts and simulated for several scenarios within each mission framework.

The first step towards analysis of the problem has been to establish the most basic analytical foundation for the implementation of the drag-free sensor. While it may appear mundane, this analytical foundation is crucial to developing a realistic assessment of the implementation of a DFC architecture. Since all past implementations of DFC technology have involved the design of a spacecraft *around* the drag-free sensor, many of these details have been ignored. While it is feasible to design a constellation around a DFC concept, it is not feasible to design a spacecraft around a DFC sensor, because there is no scientific, operational scenario where the DFC sensor will be the “payload” and such a sensor must be a secondary, supporting device, not the center of attention. Henceforth, Section V details some of the historical work as well as our establishment of the core analysis for practical implementation of a DFC system. It begins to draw the boundaries of applicability for a DFC system under the real constraints, including the fact that during the design and development process, a spacecraft center of gravity (cg) will move substantially and it is not feasible to require that such a sensor be positioned at the cg. Therefore, a key element in the analysis is the understanding of what the impacts on cg offset will be.

Technical Objectives

1. Develop an optimal control correction algorithm to ensure uniform consumption of fuel over the spacecraft constellation and subsequently determine the overall fuel consumption for such an architecture.
2. Compare the fuel consumption to a traditional approach of allowing each satellite’s orbit to decay for 2-4 weeks and applying a Δ -V correction.
3. Compare and contrast this approach for handling the 30 spacecraft control problem to traditional means based on extensions of single spacecraft control approaches.
4. Determine a break-even point where the number in the constellation is large enough to indicate that such an option is cost effective (even if the number is determined to be 1).

5. Compare the effects of drag-based constellation decay vs. effects due to the earth-oblateness perturbation. This will help to establish for which orbital altitudes and inclinations the drag-free method has substantial payoff.

IV. History and Future of Drag-Free Control

Drag-free Control of a spacecraft was initially proposed in the 1960's and is discussed extensively by Lange.¹ A free-floating proof mass is enclosed within a spacecraft, isolating it from external disturbance forces such as atmospheric drag and solar radiation pressure. Under ideal conditions, internal disturbance forces can be ignored, and the orbit of the proof mass will depend only on gravitational forces. Using small thrusters, the spacecraft can be forced to follow the orbit of the proof mass, thus counteracting any non-gravitational disturbance forces.

The first drag-free control system was flown in 1972 as part of the Navy's TRIAD mission.² The purpose of this experimental mission was to improve the predictability of spacecraft navigation by eliminating external disturbance forces on the spacecraft. To that end, a 3-axis Disturbance Compensation System (DISCOS) was developed and tested on TRIAD. A single-axis version of the TRIAD DISCOS was subsequently used on another Navy spacecraft, NOVA-1.³ The purpose of NOVA-1, like that of TRIAD, was to improve the predictability of the spacecraft ephemeris. Additional uses for drag-free control have been proposed and include gravitational field measurement (Gravity Explorer Mission), equivalence principle testing (Gravity Probe B), and gravitational wave measurement (LISA).⁴ It is important to note that in the context of Space Science missions such as LISA and GPB, the concept of "drag-free" takes a broader context in that drag now refers to solar radiation pressure, solar winds, and other such external pressure effects that do not necessarily act against the vehicle velocity.

Because of the stringent acceleration requirements on the drag-free missions currently in design or operation, it is very important to minimize errors due to internal disturbances such as mass attraction, radiation pressure, magnetic field gradients, and electrostatic charge. Therefore, in each of the drag-free spacecraft designed to date, the spacecraft was designed around the drag-free sensor package. In essence, the drag-free sensor package is the principle spacecraft payload.⁴ Designing the spacecraft in this manner helps to minimize the internal disturbance forces, which allows the proof mass within the drag-free sensor to follow an ideal, gravitational orbit very closely, thus allowing for better elimination of the external disturbance forces acting on the surrounding spacecraft without a substantially challenging sensing problem. The disadvantage of this method of design is that it results in a higher degree of difficulty in designing the spacecraft. Any small change in the hardware, for example, can result in a shift of the spacecraft center of mass. This shift of the center of mass can then result in an unacceptable bias of the drag-free sensor. The effects of a center of mass shift on the drag-free sensor are discussed later in this paper.

Despite the difficulties in designing a drag-free spacecraft, drag-free control is still a desirable means of spacecraft control in certain cases. In low Earth orbit, atmospheric drag causes the greatest uncertainties in predicting spacecraft ephemeris. The continuously varying atmospheric

drag levels require increased spacecraft tracking in order to accurately predict spacecraft location. In addition, periodic propulsive maneuvers must be performed to counteract the effects of drag on the spacecraft orbit. If the effects of drag on the spacecraft orbit can be autonomously counteracted through the use of a drag-free control system, the uncertainty of atmospheric drag is essentially eliminated from the spacecraft flight dynamics equation. With the elimination of drag, the main perturbations acting on the spacecraft orbit are the perturbations due to the Earth's gravitational field, which are easily predicted.

As was mentioned before, the difficulty in designing the current drag-free spacecraft occurs because of the stringent acceleration requirements for the various drag-free missions. With looser requirements, it could be possible to design a simple, drag-free system that can be added to a LEO spacecraft to enable autonomous orbit control. The drag-free sensor continuously monitors the position of the proof mass with respect to the surrounding spacecraft. Based on the proof mass position, small thrusters are fired to move the surrounding spacecraft such that the proof mass stays centered within the spacecraft. This control of the proof mass position continuously counteracts the effects of drag on the spacecraft orbit by forcing the spacecraft to follow the proof mass orbit. This continuous drag compensation decreases the spacecraft tracking required, thus reducing the number of people needed for ground station staffing. It also allows for fewer large orbit correction maneuvers, which reduces the need for extra staff to plan and execute periodic orbital maneuvers.

In order to determine the viability of continuous drag-free control, the benefits mentioned above must be weighed against the costs. This section of the report discusses the theoretical cost of using continuous drag-free control to compensate for the effects of drag on a spacecraft in low Earth orbit. This cost will be considered in terms of cumulative orbital velocity changes, or ΔV , and is in comparison to a traditional approach of allowing the spacecraft's orbit to decay for two to four weeks and applying a larger ΔV correction.

V. ΔV Simulation

Of interest in this study is the total ΔV required for continuous drag compensation as compared to the ΔV required for periodic drag compensation. To determine the ΔV requirements, a simulation was created using a combination of MATLAB and the Astrogator module within Satellite Tool Kit (STK). The Mission Control Sequence (MCS) of the simulation consists of the Spacecraft Initial Conditions, the Propagator, and a Target Sequence. Within the Target Sequence is an Impulsive ΔV Maneuver. The Propagator includes two-body gravitational effects and the Jacchia-Roberts atmospheric density model. The simulation, therefore, calculates only the ΔV required to counteract atmospheric drag effects. The Jacchia-Roberts parameters chosen are daily and average F10.7 values of 150 W/m^2 and a geomagnetic index number of 3.0. The F10.7 values were chosen to represent an average solar flux.⁶

At the beginning of each simulation case, MATLAB updates the spacecraft orbital elements in STK using initial conditions stored in the MATLAB script. STK propagates the spacecraft orbit over a time step, Δt . The Target Sequence then calculates the ΔV required, when applied along the spacecraft velocity vector, to raise the spacecraft semi-major axis to within 10 cm of its original value. Only the velocity vector is targeted because atmospheric drag always acts

Table V-1: Summary of initial spacecraft parameters for the simulation.

Initial Spacecraft Parameters		
		Value/Range
Altitude	Varies	350 - 700 km
Inclination	Varies	0 - 60 deg
Ballistic Coefficient	Varies	25 - 200 kg/m ²
Eccentricity	Fixed	0
RAAN	Fixed	0 deg
Argument of Perigee	Fixed	0 deg
True Anomaly	Fixed	0 deg

opposite the spacecraft velocity. The Impulsive Maneuver then applies the ΔV along the spacecraft velocity vector. It is assumed at this point that the ΔV can be applied exactly along the velocity vector, and therefore there are no ΔV losses due to attitude error. MATLAB then takes the spacecraft orbital elements at the end of the Impulsive Maneuver and uses them to update the orbital elements in STK. MATLAB also records the calculated ΔV . This cycle continues until the spacecraft has been propagated through a total of four weeks. A flowchart of the STK/MATLAB simulation can be seen in Figure V-1.

A total of four parameters affecting drag were varied to establish the different simulation cases studied: orbit altitude and inclination, spacecraft ballistic coefficient, and the time between ΔV maneuvers. Table V-1 shows a summary of the initial spacecraft parameters for the simulation. The ballistic coefficient is the spacecraft mass divided by its cross-sectional area times the drag coefficient. A drag coefficient of 2.0 was assumed for all cases. Values for the ballistic coefficient were chosen based on information from past spacecraft² and are assumed to be constant throughout the four-week propagation/ ΔV maneuver cycle (*i.e.* mass and cross-sectional area of the spacecraft are assumed to be constant).

The simulation time steps, or the time between ΔV maneuvers, varies from four weeks to one

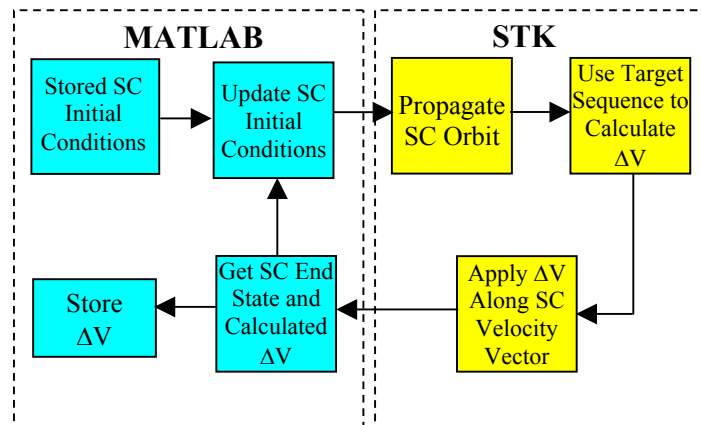


Figure V-1: Flow chart of STK/MATLAB Simulation

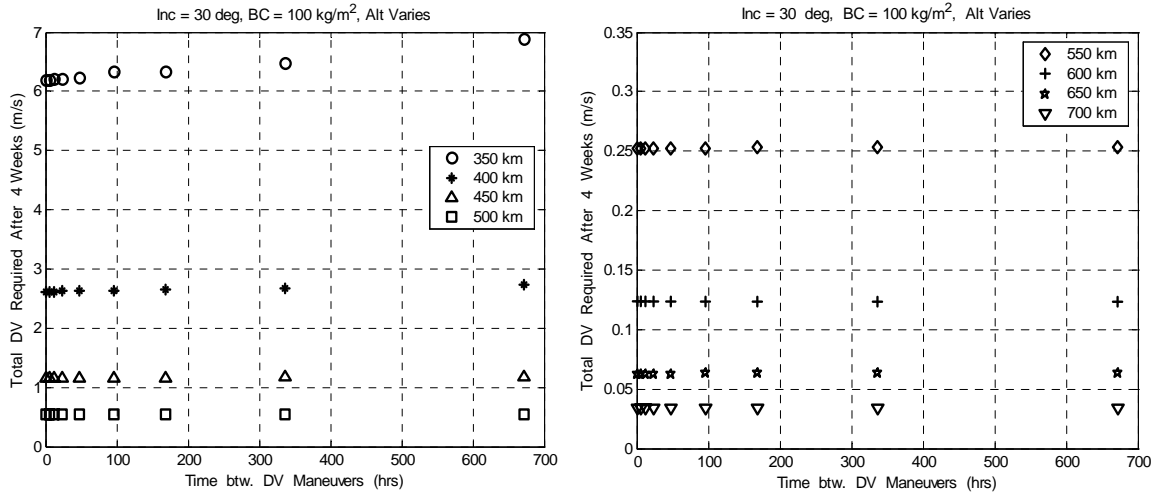


Figure V-2: ΔV curves for all altitudes at an inclination of 30° and a ballistic coefficient of 100 kg/m^2

hour. The four-week and two-week time steps are representative of the time between traditional periodic orbit correction maneuvers. The one-hour time step is more representative of continuous drag compensation. Additional time steps tested were one week, four days, two days, one day, twelve hours, and six hours. These intermediate time steps were simulated to show the general trend in the ΔV required as the control approaches continuous compensation.

Simulation Results

Recall that varying three spacecraft parameters and the time between ΔV maneuvers were used to specify the different cases of the simulation. A total of 448 cases were run for each of the nine different ΔV time steps, for a total of 4032 cases. Based on the data, several overall trends can be noted. First of all, in all the cases simulated, there is no extra ΔV required for the one-hour ΔV maneuvers as compared to the two or four-week maneuvers. In fact, in some cases there is even a significant savings with the one-hour maneuvers.

The cases with the largest ΔV savings are at low altitudes and low ballistic coefficients. This

Table V-2: Comparison of ΔV required at different altitudes and ballistic coefficients.

ΔV Comparison for Different Ballistic Coefficients (m/sec)			
BC (kg/m^2)	1 Hour ΔV Separation		
25	24.64	2.13	0.13
100	6.19	0.53	0.03
200	3.10	0.27	0.02
	350	500	700
	Altitude (km)		
	Inclination = 30 deg		

result is not surprising since the acceleration due to atmospheric drag increases proportionally with a decrease in ballistic coefficient and increases exponentially with an increase in atmospheric density, which increases exponentially with decreasing altitude. The altitude of a spacecraft with a low ballistic coefficient in a low orbit will decrease at a faster rate than a spacecraft with a higher ballistic coefficient in a higher orbit. Therefore, it will require less total ΔV to raise the semi-major axis after every hour, for four weeks, than it will to raise the semi-major axis at the end of four weeks. At higher ballistic coefficients and higher altitudes, this effect is reduced, and therefore ΔV savings decrease.

At altitudes above 400 km, there does not appear to be any significant difference between the ΔV required for the four-week maneuver and for four weeks of one-hour maneuvers. This trend holds true at all inclinations and ballistic coefficients and can be seen in the example cases in Figure V-2. The slopes of all lines above 400 km are approximately zero, indicating little to no extra ΔV cost for continuous drag compensation.

Another interesting trend in the data is the effect of the ballistic coefficient on the ΔV curves. Recall that the ballistic coefficient is the ratio of the spacecraft mass to its cross-sectional area times the coefficient of drag, and as such has a direct effect on the total amount of ΔV required. The effect of a lower ballistic coefficient is an increase in drag. This increase in drag then requires larger amounts of ΔV for drag compensation. This trend holds true at any altitude and is represented in Table V-2.

Of interest is also the effect of the ballistic coefficient on the slope of the ΔV curve. As can be seen in Table V-2, at altitudes of 400 km and above, at any inclination, the slopes of the ΔV curves for different ballistic coefficients are approximately equal. This trend implies that the cost differences between periodic and continuous drag compensation are similar for all ballistic coefficients. At lower altitudes, the slopes of the ΔV curves vary from one ballistic coefficient to another, implying that different ballistic coefficients have different effects on the ΔV cost between periodic and continuous drag compensation. This trend can be explained in that drag lowers the altitude of a spacecraft with a low ballistic coefficient at a faster rate than a spacecraft with a high ballistic coefficient. So, as the time between ΔV maneuvers decreases, the total ΔV required after four weeks will decrease at a faster rate for a spacecraft with a low ballistic coefficient than for a spacecraft with a high ballistic coefficient.

The final interesting trend from the simulation data is the effect of orbit inclination on the ΔV cost curve. The initial inclination of the spacecraft orbit appears to have a very slight effect on the total ΔV required for drag compensation and no effect on the slope of the ΔV curve. This trend holds true for any given altitude and ballistic coefficient. This relative insensitivity to orbit inclination is not surprising considering that drag depends predominantly on spacecraft altitude and exposed area. The slight increase in ΔV required at low inclinations can be explained by an increase in average atmospheric density for a given orbital semi-major axis, which is associated with the oblateness of the Earth at the equator.

In summary, Table V-3 shows the ratio of Continuous/Periodic ΔV required, per year, for drag compensation of a spacecraft at various altitudes and ballistic coefficients. As was pointed out earlier, the inclination of the spacecraft orbit has little effect on the amount of ΔV required; therefore, these approximations are valid for all inclinations. The periodic compensation in this calculation is taken to be every four weeks.

VI. Errors due to Center of Gravity Assumption

A potentially significant source of error in the simulation data comes from the assumption that the proof mass is located at the center of gravity (cg) of the spacecraft. In actuality, it is not always possible to place the proof mass exactly at the spacecraft cg. The location of other components or component wiring issues could require that the proof mass be offset slightly from the spacecraft cg. In addition, the spacecraft cg has a tendency to shift throughout a mission from fuel usage, outgassing, *etc.* The following subsections will discuss in detail the effects of small offsets of the proof mass from the spacecraft cg.

The flight heritage, and future flight planning, of drag-free technology has been in missions for which the proof mass sensor is a primary function. Therefore, the goal of maximizing efficacy of the drag-free sensors has dominated design considerations. In particular, these missions have endeavored to place the proof mass target point very close to the spacecraft cg. In his treatment of the drag-free satellite concept in 1964¹, Lange mentions the bias caused by a cg offset, and

Table V-3: Summary of the ratio of Continuous/Periodic ΔV requirements, per year, for drag compensation of a spacecraft.

Ratio of ΔV Requirements: Continuous / Periodic Drag Compensation								
	Altitude (km)							
Ballistic Coefficient (kg/m ²)	350	400	450	500	550	600	650	700
25	0.47	0.83	0.93	0.97	0.99	0.99	1.00	1.00
50	0.78	0.92	0.97	0.99	0.99	1.00	1.00	1.00
75	0.86	0.95	0.98	0.99	1.00	1.00	1.00	1.00
100	0.90	0.96	0.98	0.99	1.00	1.00	1.00	1.00
125	0.92	0.97	0.99	0.99	1.00	1.00	1.00	1.00
150	0.93	0.97	0.99	0.99	1.00	1.00	1.00	1.00
175	0.94	0.98	0.99	1.00	1.00	1.00	1.00	1.00
200	0.95	0.98	0.99	1.00	1.00	1.00	1.00	1.00

approximates the bias magnitude as g (gravity at the Earth's surface) times the ratio of the cg offset to the orbit radius, which ratio he gives as 10^{-10} – 10^{-11} . This estimate would indicate a displacement of 0.1–1 millimeter for a 700-km altitude; this implies the spacecraft has been carefully designed around the drag-free sensor package. Lange points out that, for low-Earth orbits, the drag acceleration averages 10^{-4} – $10^{-8}g$, and so is much greater than that required because of the cg offset.

Lange was concerned with showing that drag-free control was a feasible concept, and therefore could expect a careful design process to minimize the displacement of the proof mass from the satellite cg. However, some current efforts have as a goal the expansion of drag-free sensor technology to multiple uses. For a generic drag-free sensor to become a practical addition to the spacecraft design toolbox, the placement of the sensor would need to be much less restricted than the sub-millimeter, or even the centimeter level, allowing the sensor to be used in missions where the drag-free component is not the primary driver of design considerations.

In this paper are discussed the effects that may be expected if a generalized drag-free sensor is placed some distance away from the spacecraft cg. The proof mass will follow a relatively unperturbed gravitational trajectory. If the proof mass enclosure were placed at the spacecraft cg, then the gravitational trajectory of the spacecraft would be identical to that of the proof mass. All propulsive effort would go to achieving and maintaining a drag-free state; this effort would be necessary whether drag-free technology were used or not. However, a separation between the proof mass and the spacecraft cg can cause a relative acceleration between the two bodies due solely to gravity. This acceleration would have to be countered in addition to the drag forces, and so maintaining function of the drag-free sensor would require additional propulsion that would not be needed if the drag-free sensor were absent.

This cg offset effect occurs even in the strictly Keplerian, two-body dynamics, and it is unrelated to the microgravity (*i.e.* self-gravity) bias accelerations mentioned above. In many cases, the additional propulsive effort would be significant in relation to total propulsive costs; the continuation of this paper explores the factors that will help determine when the additional costs are restrictive.

The first-order effects of cg offset are easily derived from elementary force-balance principles, but their formulation is dependent upon the spacecraft orbit/attitude profile, *e.g.* inertially fixed, Earth-pointing, *etc.* Lange provides an approximation for the additional force required to maintain a cg offset. What follows here is a more specific derivation of the first-order effects on an Earth-pointing satellite in a circular orbit. This derivation may be modified to suit other orbit/attitude profiles or adapted to allow 6-degree-of-freedom dynamical modeling. A spherical Earth with gravitational constant μ and perfect attitude/orbit maintenance are assumed.

Consider a free-floating proof mass (index \mathbf{P}) in a circular orbit of radius, \mathbf{R}_P , with circular orbit velocity,

$$v_P = \sqrt{\frac{\mu}{R_P}}. \quad (1)$$

The host satellite (index \mathbf{S}) maintains positioning such that the proof mass is located at the center of its sensor cage, where the sensor cage is offset below the spacecraft cg by a radial

displacement, d . Due to the Earth-pointing attitude profile, the spacecraft cg keeps the same angular rate as the proof mass, but follows a circle of radius,

$$R_S = R_P + d. \quad (2)$$

To maintain that angular rate, the spacecraft must have a greater linear velocity than the proof mass, given by

$$v_S = \frac{R_S}{R_P} v_P = \frac{R_P + d}{R_P} v_P. \quad (3)$$

However, the circular orbit that the satellite is following has a different Keplerian circular velocity associated with it:

$$v_{circular} = \sqrt{\frac{\mu}{R_P + d}}. \quad (4)$$

This velocity is less than that which the satellite must maintain to avoid contacting the proof mass. To remain in circular orbit at super-circular velocity, a constant acceleration must be applied in the radial direction so that the centripetal acceleration of the satellite guides it along the correct trajectory. This acceleration, Δa , is given by subtracting the gravitational acceleration, a_g , from the necessary centripetal acceleration, a_c :

$$\Delta a = a_c - a_g = \frac{v_S^2}{R_S} - \frac{\mu}{R_S^2}. \quad (5)$$

The fact that any displacement, d , must necessarily be much smaller than the orbit radius implies $R = R_P \approx R_S$. Substituting from Equations 8–10 and keeping only the first-order terms in d gives the simplified expression

$$\Delta a \approx \frac{3\mu d}{R^3}. \quad (6)$$

This equation approximates the additional acceleration, beyond any used to cancel drag and similar effects, required for an Earth-pointing satellite to follow a proof mass with a radial cg offset. Other potential displacement-plus-dynamics combinations are simple to analyze. If the displacement is along the velocity direction, then to first order the proof mass is in the same orbit as the spacecraft with a different true anomaly, so there are no strong effects. If the displacement is in the cross-track direction, the expression is similar, with the multiplier of 3 changing to $\sqrt{2}$:

$$\Delta a \approx \frac{\sqrt{2}\mu d}{R^3}. \quad (7)$$

And, if the attitude profile is inertial, instead of Earth-pointing, the acceleration in Equation 6 is reduced by a factor of two-thirds, and the effect over a single orbit is sinusoidal in the inertial frame, with an orbit average equal to zero. However, to be able to ignore the effect, the cg would have to be inside the sensor cage, with enough clearance that the proof mass could revolve about the cg at distance d . Since proposed sensing designs (*e.g.* capacitive or optical) may require close proximity between the proof mass and its enclosure, such clearances would not be feasible in those cases.

Implications of Center-of-Gravity Offset

The potential effects of cg offset are easy to calculate for any given mission, once the mission design and integration has been completed and the mass properties determined. However, to

place a drag-free sensor at the cg of a spacecraft by design, and have the cg be exactly where it was intended at the end of integration requires considerable effort and expense. A cg offset would require more fuel than the same mission with no drag-free sensor, and the fuel increase would be proportional to the size of the offset. Fuel requirements are a major driver in early design concepts, and the risk associated with possible cg offsets would become a factor weighing against the use of drag-free sensing. Another consideration is that the use of fuel over a mission lifetime will likely move the cg within the spacecraft, and the effects of the resulting offset must be acknowledged as the basic structural design is being developed.

It should be recognized, however, that the cg-offset effects are limited to additional fuel expenditures. In the case of other drag-free biases, the satellite may be led gradually to raise or lower its orbit due to a constant bias force along the drag direction, as the proof mass is pulled or pushed along the velocity direction. By contrast, the cg-offset effects do not act on the proof mass at all, so though additional fuel is used, the proof mass orbit—and therefore the predictability desired from drag-free control—is maintained.

An example of how a cg offset can affect a mission will provide better insight into the issue. The TRIAD-1 satellite, launched in 1972 as part of the Navy TRANSIT program, provides a good illustration of how cg offset can affect a mission.² The satellite experienced a small malfunction in the deployment of its booms, resulting in one of two 2.7-meter booms being under-extended by an estimated 1 centimeter; as a consequence, the proof mass null point was displaced radially from the spacecraft cg. Therefore, when the satellite was flown in a closed-loop, drag-free mode, the predominant observed disturbance was a bias in the radial direction of about $3\text{--}5 \times 10^{-9}$ g, as opposed to the expected maximum bias levels of about 10^{-11} g from self-gravity and electrostatic charging effects. The TRIAD-1 team did identify the problem as being due to cg offset, but was “surprised” by the magnitude of its effect.

Comparison of Offset Effects with Drag

The deceleration of a satellite due to atmospheric drag is given by

$$a_D = \frac{1}{2} \rho v_S^2 C_B \quad (8)$$

where ρ is the atmospheric density, v_S is spacecraft velocity, and C_B is the ballistic coefficient. Here, this ballistic coefficient is defined as the ratio

$$C_B \equiv \{\text{vehicle mass}\} : \{\text{drag coeff.} \times \text{drag area}\}.$$

It is well known that atmospheric density increases at an exponential rate as altitude decreases. The drag force increases even more with decreasing altitude, since the orbital velocity increases as a satellite approaches the Earth. From Equation 13, it may be seen that the idealized cg offset effect also increases with decreasing altitude, but only as the cube of the orbit radius. Therefore as altitude decreases, there is a crossover altitude for any given combination of ballistic coefficient, C_B , and cg offset, d , at which the magnitudes of the two effects—drag and cg offset—are equal. Thus, satellites above the crossover altitude would be spending more fuel for compensation of their cg offset than for drag compensation. To illustrate the principle for an Earth-pointing vehicle with $C_B = 100 \text{ kg/m}^2$ and $d = 10 \text{ cm}$ in the radial direction, the crossover

altitude is just under 450 km (based on the mean densities provided by Larson & Wertz⁶). This example represents a typical satellite. Smaller satellites tend to have smaller mass-to-area ratios, and at the same time could more easily have the drag-free sensor close to the cg. A microsatellite might therefore be better described by a C_B of 25 kg/m² and a cg offset d equal to 1 cm; such a satellite would have a crossover altitude of about 700 km.

As an example of a potential systems trade that this cg offset effect could drive, consider a mission where the engineering determination is made that for a 400-km altitude and a C_B of 200 kg/m² (typical for medium- to large-sized satellites), the final offset must be small enough that its effect is less than 5% of the drag acceleration. The maximum allowable radial offset would then be about 5 cm. This is not as restrictive as it might first seem, as the sensor could be placed on the front or back of the spacecraft, so long as the radial offset were less than 5 cm and the cross-track offset less than 10 cm (from Eq. 14). This restriction is not prohibitive, but ample consideration early in the design process would be necessary. Figure 1 illustrates the trade space more fully by comparing the effects of drag with the additional acceleration due to cg offset for several ballistic coefficients and cg offsets.

As the cg offset d increases, so will ΔV_{error} . Table VI-1 shows some calculated values for $\ddot{\mathbf{r}}_{error}$ and ΔV_{error} , assuming a positive 10 cm offset. The final two columns show the ΔV calculated by the simulation assuming ballistic coefficients of 25 kg/m² and 100 kg/m². As can be seen in the table, the errors due to an offset proof-mass become increasingly significant as drag forces decrease sharply with increasing altitude and as the ballistic coefficient increases. In these cases, it becomes just as expensive to compensate for the errors due to proof-mass offset as it is to compensate for drag on the spacecraft.

Table VI-1: Estimated errors due to proof-mass offset from the spacecraft center of gravity. The final columns show the ΔV calculated in the simulation at ballistic coefficients of 25 kg/m^2 and 100 kg/m^2 as a comparison.

Errors for a 10 cm Proof Mass Offset Along Spacecraft CG Vector				
Altitude	Acceleration Error	ΔV_{error}	ΔV_{sim} (BC=25)	ΔV_{sim} (BC=100)
(km)	(m/s^2)	(m/s/ 4 weeks)	(m/s/ 4 weeks)	(m/s/ 4 weeks)
350	-2.618E-07	-0.633	53.607	7.060
400	-2.560E-07	-0.619	12.725	2.770
450	-2.504E-07	-0.606	5.022	1.193
500	-2.450E-07	-0.593	2.207	0.541
550	-2.397E-07	-0.580	1.024	0.254
600	-2.346E-07	-0.568	0.494	0.123
650	-2.297E-07	-0.556	0.247	0.062
700	-2.248E-07	-0.544	0.129	0.033

Fuel Consumption Conclusion

In terms of ΔV cost, continuous drag compensation of a spacecraft in low Earth orbit is a viable means of spacecraft orbit maintenance for certain cases. ΔV savings are most significant for spacecraft with low ballistic coefficients in low orbits. Above altitudes of about 450 km, there is little difference between ΔV costs for continuous and periodic drag compensation for any sized spacecraft. At altitudes of 450 km and below, spacecraft with ballistic coefficients above 100 kg/m^2 show no extra ΔV cost for continuous drag compensation. However, at altitudes above 450 km, the errors due to proof mass offset from the center of gravity become significant for all sized spacecraft. It becomes just as expensive to compensate for proof mass offset as it does to compensate for drag. The closer the proof mass can be placed to the spacecraft center of gravity, the higher the upper bound becomes on altitudes for which drag-free control is viable.

VII. Drag Free Control Effects on Navigation Accuracy

Introduction

To determine the effect of drag free control on navigation accuracy, we use an extended Kalman filter to process simulated GPS pseudorange data for circular orbits with altitudes of 250km and 450km, both with and without drag. The orbits without drag represent spacecraft performing drag free control about some proof mass. The orbits with drag represent a spacecraft that is either uncontrolled or performing infrequent periodic drag makeup maneuvers.

Procedure

1. Generate truth trajectories using AI Solutions' simulation tool, FreeFlyer, with 250km and 450km altitude circular orbits, both with and without drag. For each of these four scenarios, we generate 10 trajectories (total of 40 truth trajectories) with initial condition based on a mean initial state (see Table VII-1) plus random initial position, velocity, and drag coefficient offsets (see Table VII-2). Force modeling in FreeFlyer includes a 70×70 Earth gravity model, sun and moon gravitation, and Harris-Priester drag model with $k_{\text{flux}} = 200$. The simulations assume a 3000kg spacecraft, with drag area of 15 square meters.
2. Generate measurement data (GPS pseudoranges) using the Measurement Data Simulation Program, with measurement noise standard deviation of 2 meters, and with clock errors from a Rubidium clock, and a TCXO clock (10 different random variable seeds for each clock, see Table VII-3 for clock Allan Variance values), and no ionospheric delay (total of 2 data sets for each trajectory)
3. Use an extended Kalman filter (the GPS Enhanced Onboard Navigation System, or GEONS) to estimate the trajectories and evaluate the navigation accuracy (total of 80 GEONS runs).

Table VII-1 - Nominal state initial conditions (mean of J2000). The nominal drag coefficient is 2.0, and the initial clock bias or drift are zero.

Component	Position [m]		Velocity [m/s]	
	250km Orbit	450km Orbit	250km Orbit	450km Orbit
X	-6,430,735.4098	-6,624,652.2805	1,051.2894	1,051.2894
Y	675,809.5354	696,699.9419	-4,106.8807	-4,106.8807
Z	-1,477,720.6130	-1,521,483.8354	-6,491.3925	-6,491.3925

Table VII-2 - State initial covariance

Position Variance [m²]:	1,000.00
Velocity Variance [m²/s²]:	1.00
Drag Coefficient Variance:	0.01

Table VII-3 - Clock Allan Variance Parameters

Timing Standard	h_0	h_2
Rubidium	2×10^{-19}	2×10^{-20}
TCXO	2×10^{-20}	4×10^{-29}

Table VII-4 summarizes the GEONS navigation simulations. Each simulation is described by a *RunID* with the following format: *DF-abcde*, where; the value of *a* describes the altitude of the circular orbit, with *1* = 250km, and *2* = 450km; the value of *b* describes the drag model, with *1* = drag free, and *2* = Harris-Priester drag; the value of *c* describes the clock model used, with *1* = clock error (not included), *2* = Rubidium clock, and *3* = TCXO clock; the value of *d* describes the ionosphere model, with *1* = no ionospheric delay, and *2* = ionospheric delay modeled in

DataSim (we have omitted ionospheric delay for this study, as the bulk of the error introduced by ionospheric delay can be removed by including an appropriate model in the filter); the value of e varies to describe 10 random samples of the initial condition error, clock seed, and pseudorange measurement noise seed.

Table VII-4 - Summary of GEONS simulations

RunID	Trajectory				Clock Model	
	Altitude		Drag Model		Rubidium	TCXO
	250km	450km	None	Harris-Priester		
DF-1121*	x		x		x	
DF-1131*	x		x			x
DF-1221*	x			x	x	
DF-1231*	x			x		x
DF-2121*		x	x		x	
DF-2131*		x	x			x
DF-2221*		x		x	x	
DF-2231*		x		x		x

Results

Table VII-5 shows the navigation accuracy results for 80 GEONS simulations. The “mean of mean” values are calculated by averaging the mean error across the 10 sample ensemble at each instance in time. The “mean of standard deviation” values are calculated by averaging the standard deviation of the 10 sample ensemble at each instance in time.

Table VII-5 - Ensemble "mean of mean" and "mean of standard deviation" values for position, velocity, and drag coefficient estimation error

RunID	<u>Position Error [m]</u>		Velocity Error [cm/s]		Drag Coefficient Error	
	mean	standard deviation	mean	standard deviation	mean	standard deviation
DF-1121*	1.7547	0.8607	0.3586	0.1328	9.9947E-25	5.1372E-25
DF-1131*	1.3620	0.2315	0.3289	0.0387	1.0462E-24	2.8001E-25
DF-1221*	2.8656	1.7007	0.5982	0.2650	3.1664E-02	4.2359E-02
DF-1231*	1.8767	0.4545	0.4892	0.0788	3.4537E-02	4.2010E-02
DF-2121*	1.2074	0.5652	0.1716	0.0731	-1.5035E-26	2.6093E-26
DF-2131*	0.8687	0.1833	0.1397	0.0216	-1.7628E-26	5.8094E-27
DF-2221*	2.5943	1.8747	0.4230	0.2915	1.0047E-02	4.5433E-02
DF-2231*	0.6754	0.4080	0.1385	0.0576	1.0034E-02	4.5389E-02

Table VII-6 - Ensemble "mean of mean" and "mean of standard deviation" values for clock bias and clock drift estimation error

RunID	Clock Bias Error [m]		Clock Drift Error [m/s]	
	mean	std	mean	std
DF-1121*	0.0392	1.5589	-1.5493E-05	1.1205E-03
DF-1131*	8.2769	55.1900	1.0953E-01	1.4706E+00
DF-1221*	0.0102	1.8631	-2.3751E-05	1.1506E-03
DF-1231*	8.0856	55.1970	1.0877E-01	1.4705E+00
DF-2121*	0.0523	1.4937	-1.7745E-05	1.1150E-03
DF-2131*	650.2300	2085.0000	4.2443E-01	2.3419E+00
DF-2221*	0.0840	1.8954	-1.2494E-05	1.1553E-03
DF-2231*	650.1900	2084.9000	4.2435E-01	2.3420E+00

Figure VII-1 and Figure VII-2 show clock and state error and standard deviation for a sample simulation ensemble for the *DF-1121** simulation runs (250km, no drag, Rubidium clock). Figure VII-3 and Figure VII-4 show clock and state error and standard deviation for a sample simulation ensemble for the *DF-1221** simulation runs (250km, drag, Rubidium clock). The standard deviation is plotted as a “three-sigma” value for this data.

Figure VII-5 and Figure VII-6 show clock and state error and standard deviation for a sample simulation ensemble for the *DF-2121** simulation runs (450km, no drag, Rubidium clock). Figure VII-7 and Figure VII-8 show clock and state error and standard deviation for a sample simulation ensemble for the *DF-2221** simulation runs (450km, drag, Rubidium clock).

Navigation Error Conclusions

The GEONS simulation data shows 30-50 percent reduction in the position error when drag is removed. Clock bias and drift estimates improve slightly with the removal of drag. An unexpected result in this data is the improvement of the position and velocity error at the expense of clock error when the Rubidium clock model is replaced with a TCXO clock. This may be a sign of sub-optimal filter parameter tuning, and will be invested further.

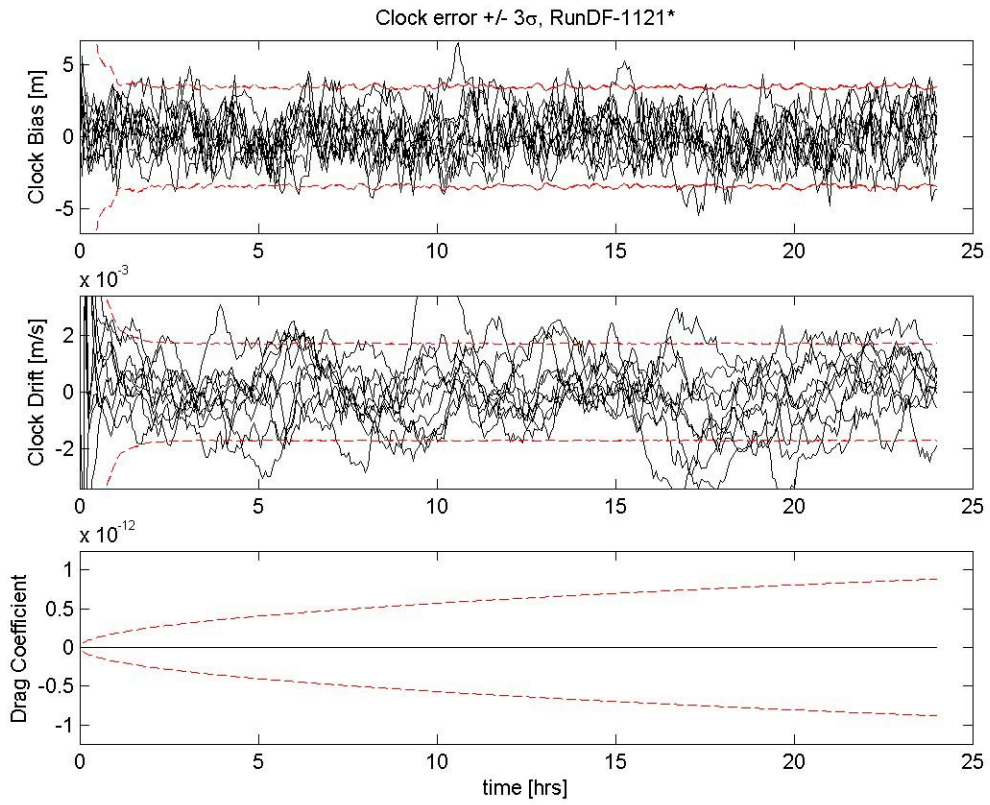


Figure VII-1 - Clock and drag coefficient errors for GEONS simulation ensemble *DF-1121**

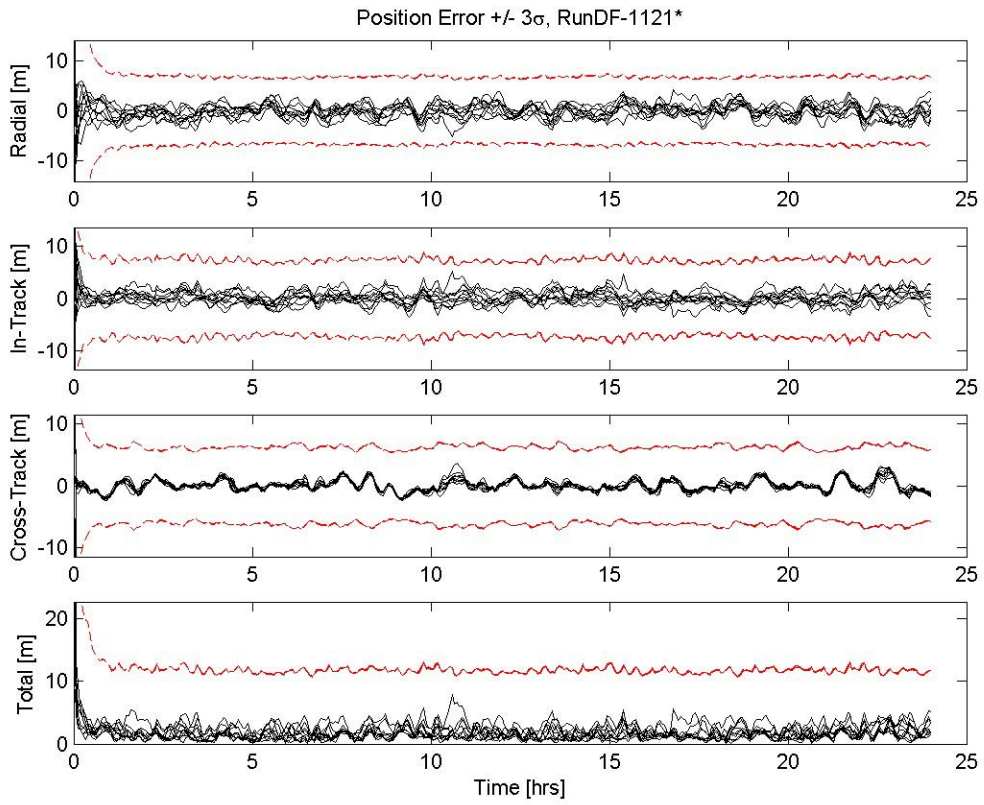


Figure VII-2 - Position errors for GEONS simulation ensemble DF-1121*

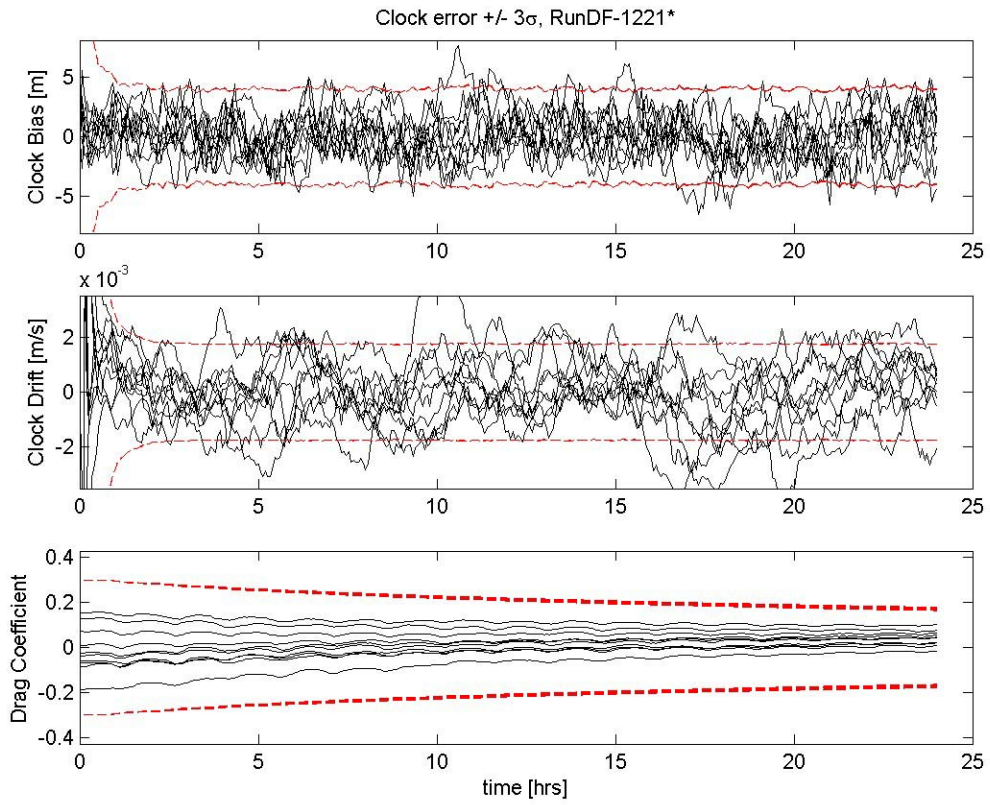


Figure VII-3 - Clock and drag coefficient errors for GEONS simulation ensemble *DF-1221**

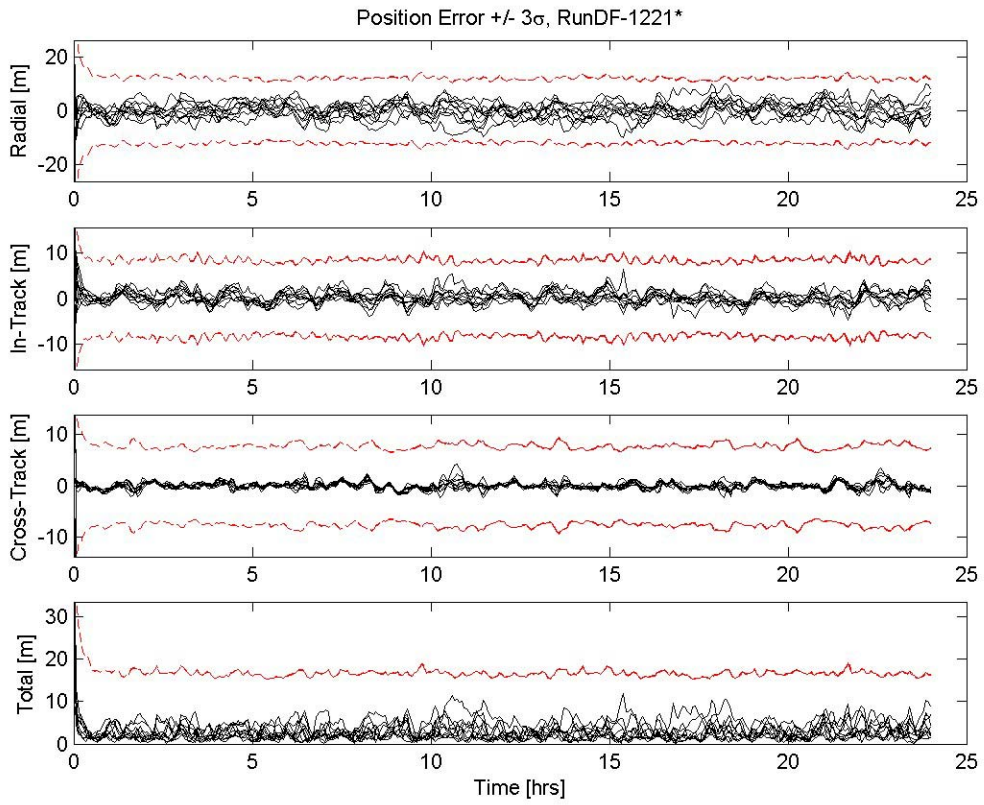


Figure VII-4 - Position errors for GEONS simulation ensemble DF-1221*

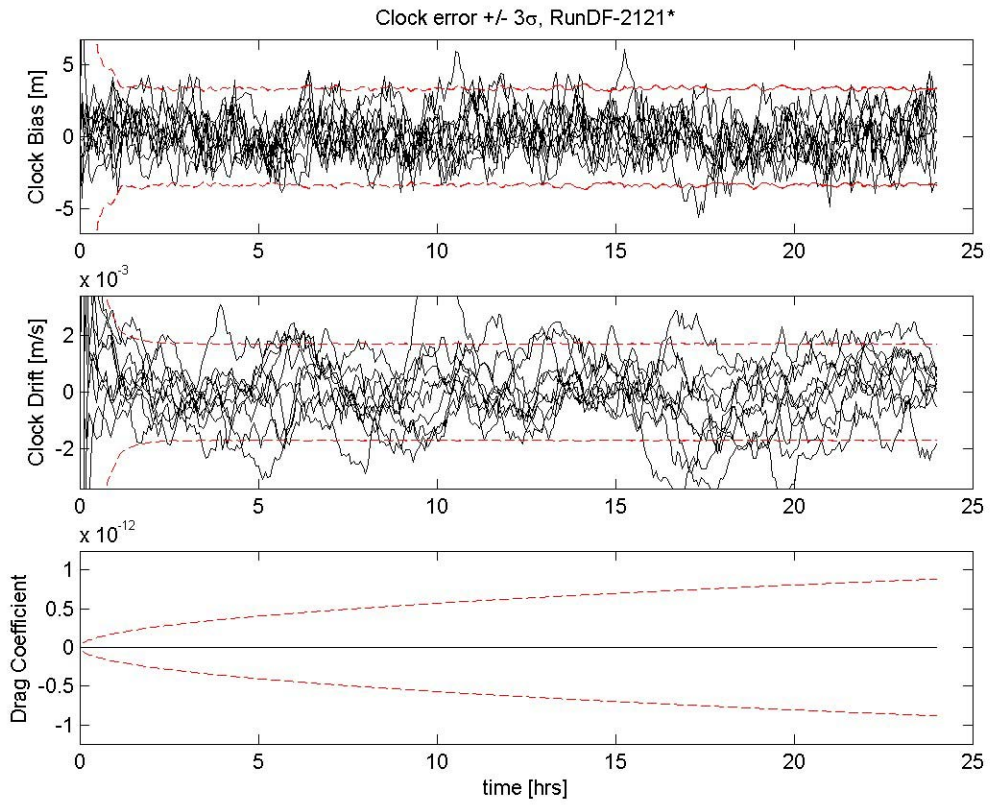


Figure VII-5 - Clock and drag coefficient errors for GEONS simulation ensemble *DF-2121**

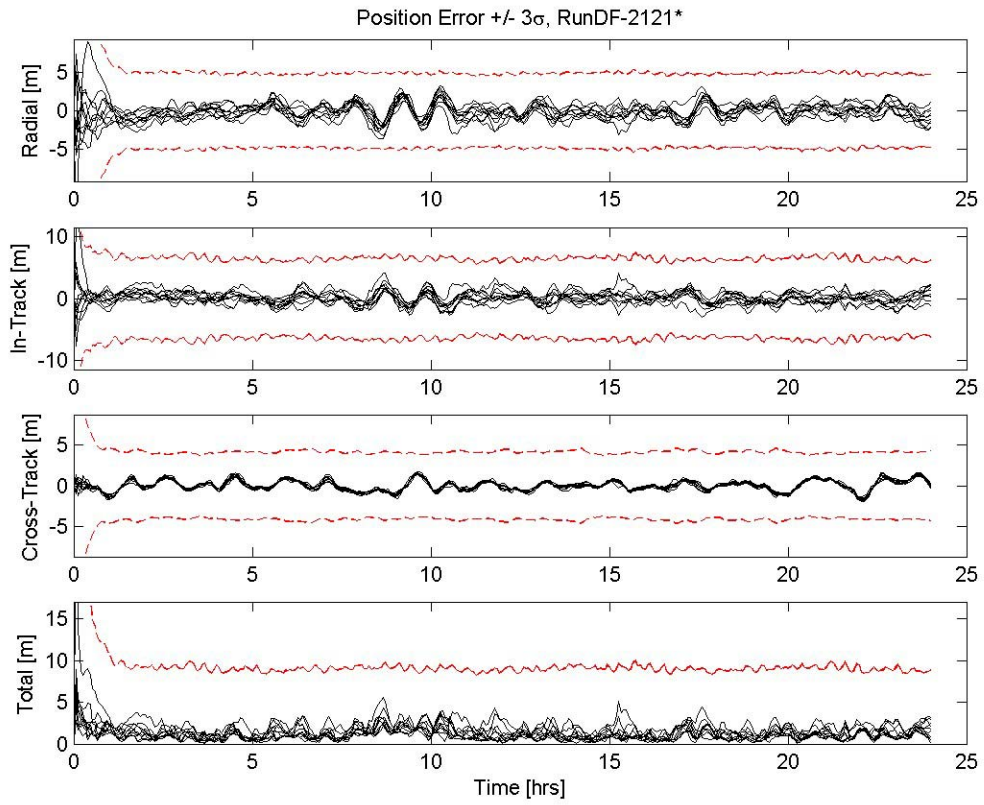


Figure VII-6 - Position errors for GEONS simulation ensemble *DF-2121**

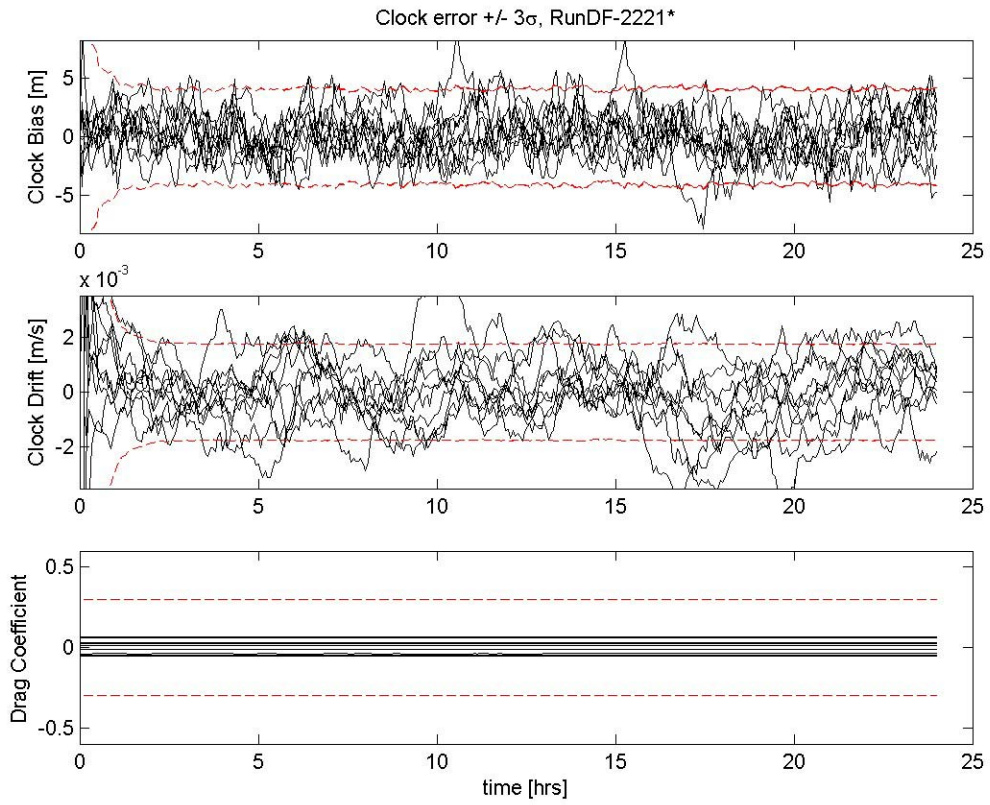


Figure VII-7 - Clock and drag coefficient errors for GEONS simulation ensemble *DF-2221**

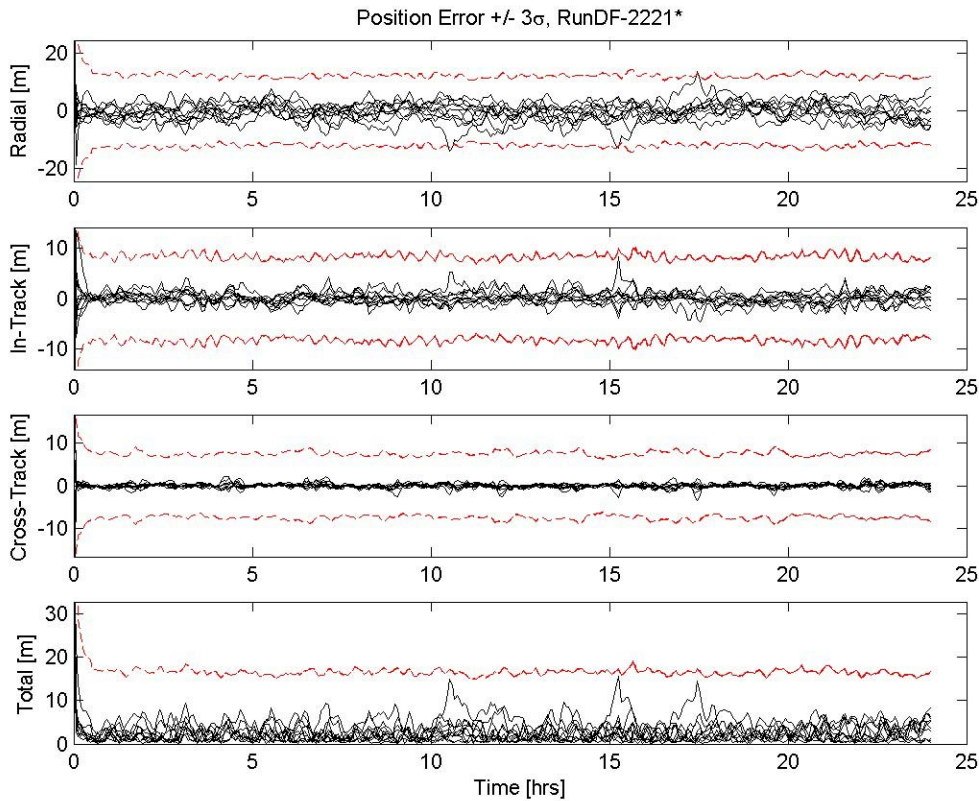


Figure VII-8 - Position errors for GEONS simulation ensemble DF-2221*

IX. Conclusions and Observations

The following list describes the conclusions and observations:

1. The use of continuous control for drag makeup (as would be required for a DFC system) is substantially more fuel-efficient than less-frequent periodic DV orbital corrections. Perhaps this appears to be an obvious conclusion but corrections due to J2 perturbation to the orbit are much more expensive when performed continuously as compared to infrequent periodic corrections. This leads to the requirement that a DFC system be considered only for constellations of satellites all in the same inclination, or more generally, in J2-invariant orbits.
2. For characteristic spacecraft in the 2000 kg class, at altitudes below 450 km, the force required to correct the drag is less than that required to correct for the cg offset. Above 450 km, the mere employment of a DFC system doubles the amount of net perturbing acceleration which must be compensated as compared to a spacecraft not employing DFC. Based on conclusion 1, this only doubles the fuel consumption if compared to a satellite whose drag is continuously compensated throughout the orbit. If the cg offset were reduced to 1 cm, this altitude crossover only increases to about 600 km, and to 1 mm would bring it to just under 800 km. Therefore, the gravitational effects really begin

to take over at an altitude of about 500 km. The effect reverses itself at extremely high altitudes (just below geosynchronous altitude), where solar radiation pressure begins to dominate over gravity. The bottom line is that for a mission higher than about 450 km, there must be substantial savings in operations cost to see a payoff for a drag-free system.

3. There is a nominal improvement of 30-50% in navigation error using GPS measurements when drag is removed from the equations of motion as is the case for the drag free system. For example the residual errors in absolute navigation are reduced from about 6 m down to 3 m assuming that the ionosphere is properly compensated, a good assumption when an advanced filter is employed such as the GPS-Enhanced On-board Navigation System (GEONS) from GSFC, or JPL's GIPSY-OASIS. The comparison is made to on-board, real-time determination accuracies, not to ground-enhanced, post-processed, differential GPS approaches, which can substantially reduce these errors in a non-real-time sense.
4. There is potential for substantial cost savings for very large constellations of spacecraft with long lifetimes if they are in a location with substantial drag effects. The determination of the payoff "knee-in-the-curve" is purely qualitative and it is based on those missions that require substantial and frequent corrections due to drag (in low altitude orbits) or solar radiation pressure (in very high altitude orbits). This can only be determined based on empirical data from the few example large constellations that exist (or existed), such as GPS, GlobalStar, and Iridium. For the case of the GPS constellation, the spacecraft are in very stable orbits, at high altitudes, and the same inclinations. Thus the corrections to orbit are due to SRP and they are performed approximately once per month. Eliminating the SRP would not substantially change the operations level of effort as most of the ground-based monitoring is for the purpose of monitoring and dealing with anomalies, with less frequent orbit corrections. The GlobalStar constellation has 48 spacecraft at 1400 km altitude with GPS on-board. GPS provides excellent time and navigation service and henceforth the operations are simple. Each spacecraft has an orbit correction (mainly due to SRP and minimal drag) about once every two months. The staff required is minimal. The Iridium Constellation does not have GPS and henceforth has a tremendous entourage required for ground support, even at the relatively high 780 km. A significant amount of this ground support is dedicated to both time corrections and orbit determination and orbit correction.
5. One of the biggest problems associated with long-term behavior of a constellation or formation is the propagation of errors in the initial conditions, in particular, the semi-major axis. The DFC constellation will still be subject to such errors and will require on-board or ground-based sensors to deal with the problem.
6. Substantial effort in optimization will be required for fuel balancing if there is significant differential drag among the spacecraft.
7. The primary competitor to this approach for autonomous control for a constellation would be a closed loop control system using GPS as a sensor. If the mission has navigation (orbit determination or position measurement) requirements, then ground

tracks, GPS, or another sensing approach will be necessary in addition to the DFC sensor. However, in either case, the closed loop architecture will be much simpler for the DFC system as compared to a closed-loop GPS-based system because there is no reliance on complex filtering schemes or the availability of GPS and the feedback is based on a simple measurement (or set of measurements) internal to the system. Likewise, such a simple control system will not be sensitive to single-event upsets, latch-ups, or other processor related issues (other than a complete failure or shutdown of the control computer).

8. While the reference spacecraft given primary consideration is a rather large 2000 kg spacecraft with ballistic coefficient of 200 kg/m^2 , strong consideration was given for microspacecraft (200 kg and less) applications. Unfortunately, there is no consistent set of statistics for microspacecraft ballistic coefficients. The certainties are that (1) the values are virtually always less than the maximum coefficients for large spacecraft, (2) there is generally little variation between the maximum and minimum values for the same microspacecraft, and (3) for large spacecraft there is frequently substantial variation between the maximum and minimum values. On the one hand, for the microspacecraft problem, all of the components are packed into a much smaller volume, henceforth with smaller wetted area for a common mass. However, it is clear after participating in spacecraft design studies for microspacecraft that one of the biggest problems is a minimum requirement for exposed area for body-mounted solar arrays to generate sufficient power. With this constraint adjoined with that of a trend of reduced spacecraft component mass, we can expect much smaller ballistic coefficients for future microspacecraft. This is not, in general, a good thing, but it does give promise for the DFC application. Furthermore, we can expect significant reduction in “travel” of the center of gravity, feasibly down to one centimeter. Henceforth, given long-term projections for microspacecraft, the domain of application can be raised as high as 700 km altitudes.
9. Viability of this approach depends on large numbers in more ways than one. In the conclusions above, it is pointed out that, operationally speaking, payoff occurs when the number of spacecraft brings operational complexity to into a substantially challenging realm. From a commercialization standpoint, this problem becomes even more extreme. Since no low-cost DFC sensor exists today, nor one designed for long-life, much technology must be developed. Without plans for development in at least the dozens, possibly the hundreds, the technology will not be affordable on a per-spacecraft basis.

X. References

¹ Lange, Benjamin, “The Drag Free Satellite,” *AIAA Journal*, Vol. 2, No. 9. Sept. 1964, pp. 1590-1606.

² Staff of the Space Department, The Johns Hopkins University Applied Physics Laboratory and Staff of the Guidance and Control Laboratory, Stanford University, “A Satellite Freed of All But Gravitational Forces: TRIAD-I,” *Journal of Spacecraft and Rockets*, Vol. 1, No. 9, Sept. 1974, pp. 637-644.

³ Eisner, A. and S. M. Yionoulis, "NOVA-1 – The 'Drag-Free' Navigation Satellite," Proceedings from the 1982 Aerospace Meeting, NASA Ames Research Center, Moffett Field, CA: 24-25 March 1982, pp. 26-31.

⁴ Vaillon, L, J. Borde, T. Duhamel, and P. Damilano, "Drag-Free Control Systems and Technologies," *Space Technology*, Vol. 16, No. 5/6, pp. 245-254.

⁵ Grabowski, Henry C., III, private communication.

⁶ Wertz, James R. and Wiley J. Larson, eds. 1999. *Space Mission Analysis and Design*, 3rd edition. El Segundo, CA, and Dordrecht, The Netherlands: Microcosm Press and Kluwer Academic Publishers.

Appendix A. Excerpt from Report on Commercial Viability

List of Acronyms

ESG	Electro-static Gyro
FOG	Fiber Optic Gyro
IR&D	Independent Research and Development
LED	Light Emitting Diode
NRE	Non Recurring (Cost)
RLG	Ring Laser Gyro
SFC	(NASA) Space Flight Center
SFIR	Specific Force Integrating Receiver
TGG	Third Generation Gyroscope
VBA	Vibrating Beam Accelerometer

Introduction

This study program with NASA Goddard SFC was undertaken to determine the feasibility of providing a cost effective sensor to enable autonomous drag free flight of satellite constellations. A parallel Honeywell IR&D project exploring theoretical concepts provided synergistic inputs for enabling methodologies discussed in Paragraphs 3.3 **Body Fixed Error Propagation vs Satellite Operating Mode** and 3.4.2.

Qualification Test Approach. These sections are considered Honeywell International proprietary and will be provided under separate cover.

Current drag free sensor technology is focused on use for extremely high accuracy gravity experiments and is consequently priced orders of magnitude higher than desired for satellite constellation use. See Figure 1.0-1 below for an example high accuracy sensor and a comparative Honeywell concept for a simpler sensor. Contacts between Honeywell and NASA identified a set of desired performance and functional characteristics for a much lower cost sensor. This report summarizes the requirements, design constraints, possible design solutions, related Honeywell technology that might be applied to production of such a sensor, and cost ranges of comparative technology for both development and production of various sensor approaches.

ONERA STAR Sensor Elements

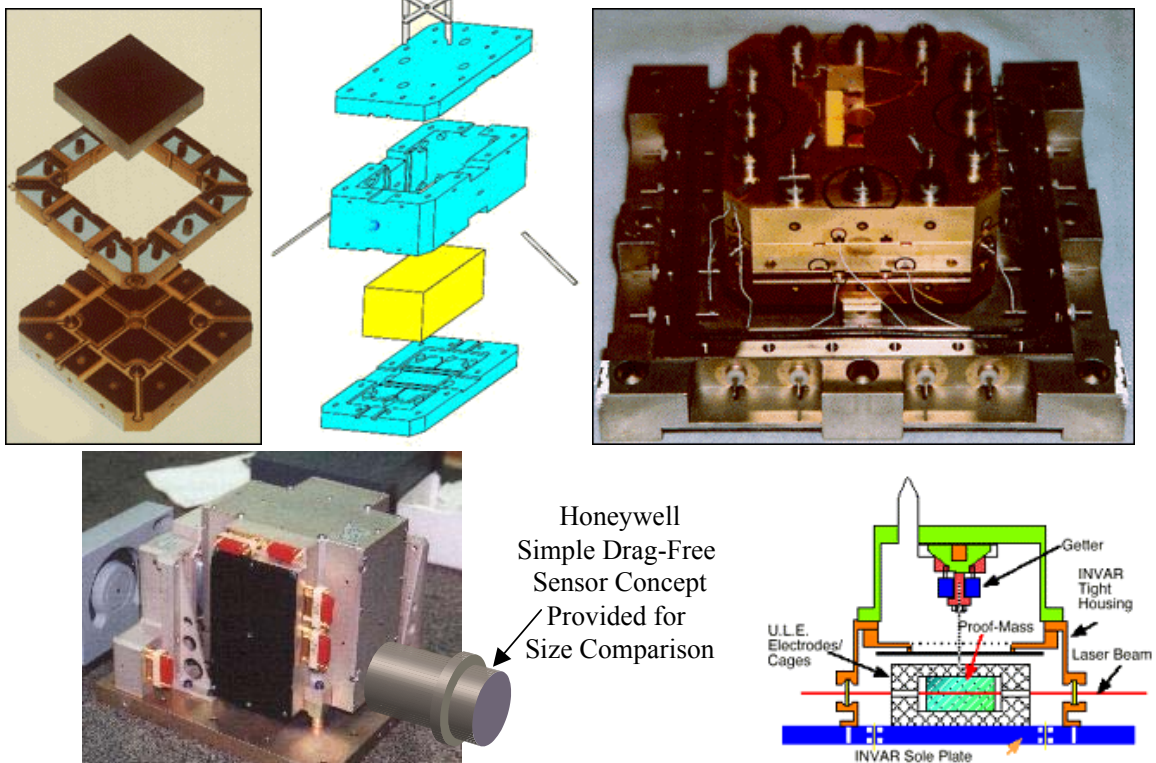


Figure 1.0-1 ONERA STAR High Precision Sensor Elements with Comparative Honeywell Concept

Requirements Summary

Since this is an exploratory program to determine the feasibility of providing a cost-effective sensor/system, no well defined requirements for the generic applications were available. In order to determine potential design solutions, a means of specifying user requirements that allowed for maximum design flexibility was needed. Utility functions were selected and after initial discussions to determine the critical sensor properties, an EXCEL based tool was provided for NASA to indicate the relative ranking and utility of each property based on their current understanding of properties needed to enable autonomous constellation station-keeping. This utility based approach allows different design approaches to achieve the same level of desirability by optimizing different properties for each design to achieve a high score.

The utility of each property is defined as the value of non-recurring engineering (NRE) development that NASA would fund to obtain the desired property. The choice of NRE as the utility tends to provide a meaningful scale of usefulness for customers to use in evaluating the value of a “to be developed” product property.

The results of the NASA ranking and utility function generation are shown in Figures 2.0-1 through 2.0-12 below.

Sensor Property	Relative Ranking	k\$ NRE (maximum utility)
Unit Price	1	\$ 2,500
Life	2	\$ 1,000
Power	3	\$ 550
Weight	4	\$ 500
Size	5	\$ 300
Reliability	6	\$ 200
Performance	7	\$ 100

Figure 2.0-1 Requirements Weighting Summary

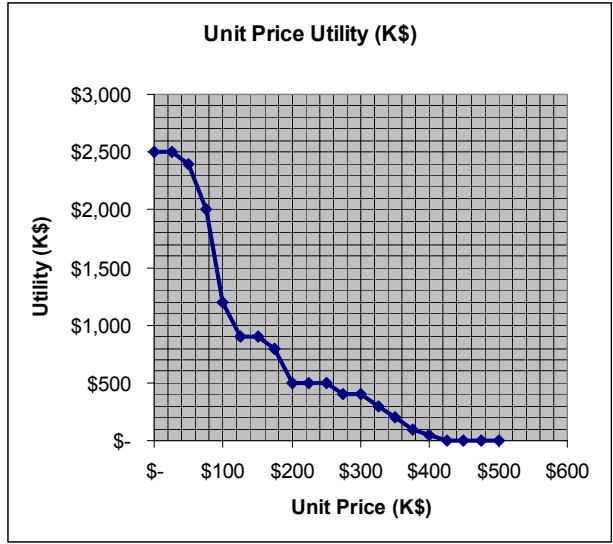


Figure 2.0-2 Price Utility

The Price Utility function indicates that the most desirable unit price is under \$20K, but that prices out to \$400K might be tolerated.

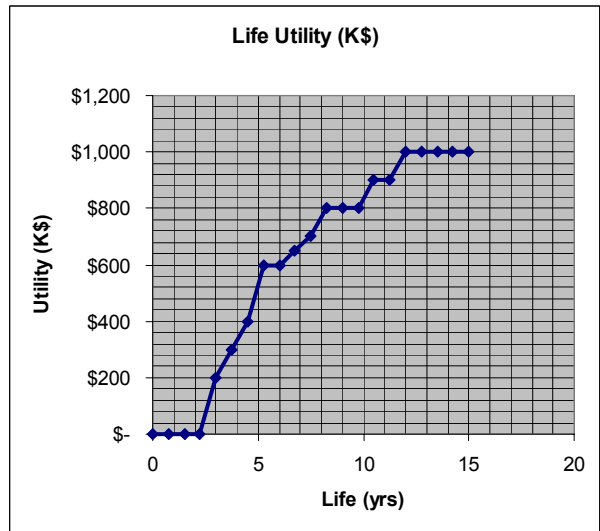


Figure 2.0-3 Life Utility

The Life Utility shows a wide range of acceptable life, ranging from 2 to 12 years with no additional value for life capability in excess of 12 years.

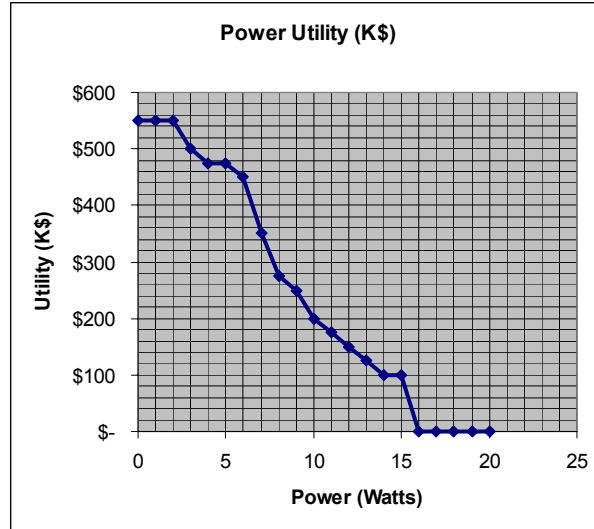


Figure 2.0.4 Power Utility

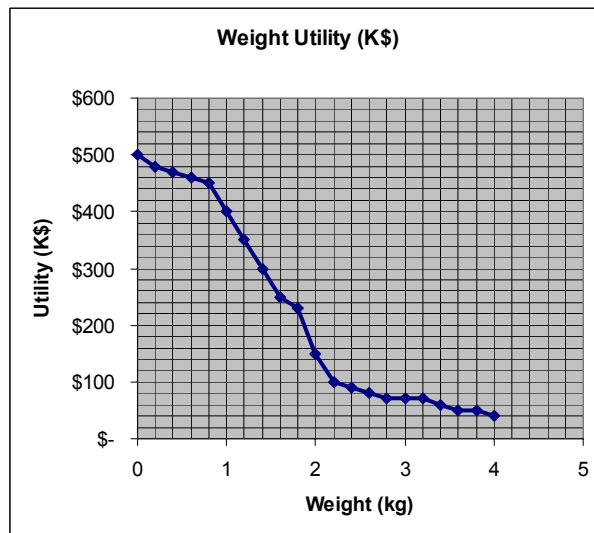


Figure 2.0-5 Weight Utility

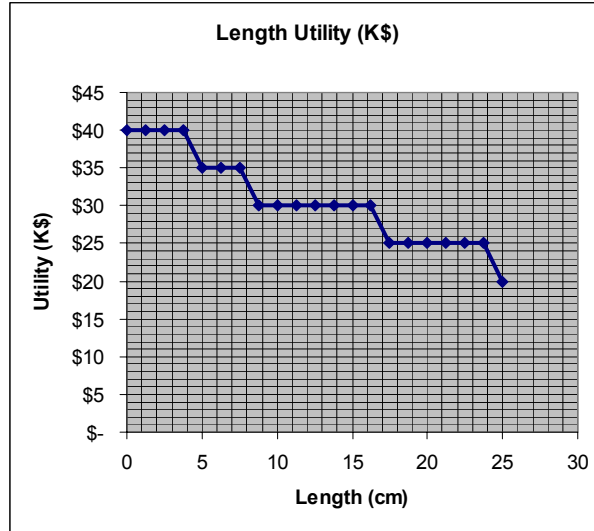


Figure 2.0-6 Length Utility

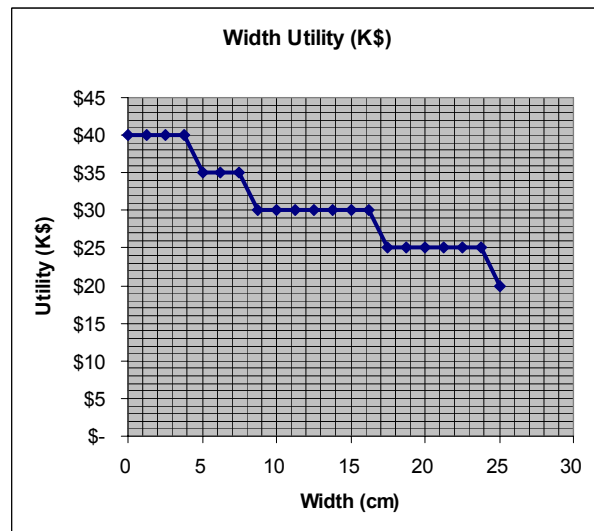


Figure 2.0-7 Width Utility

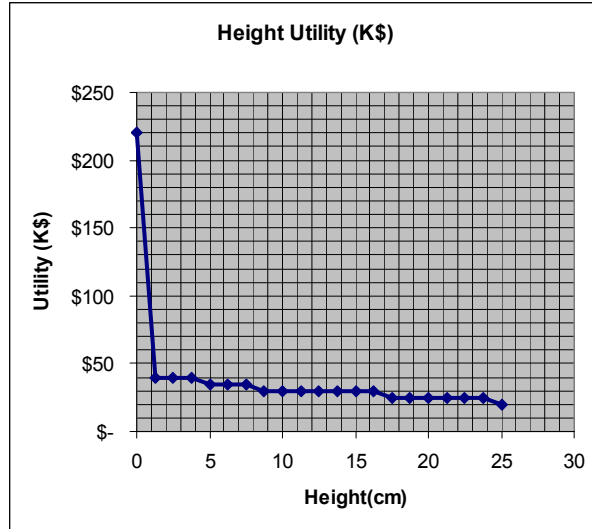


Figure 2.0-8 Height Utility

The three Size Utilities indicate a planar configuration of no more than 1 cm in height is desirable, while length and width can range up to 25cm.

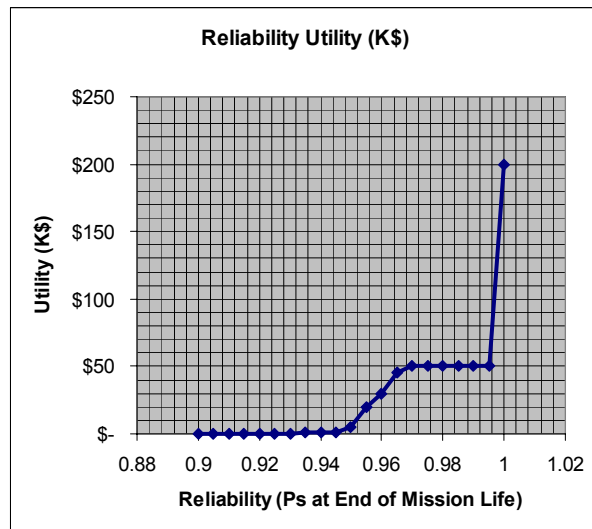


Figure 2.0-9 Reliability Utility

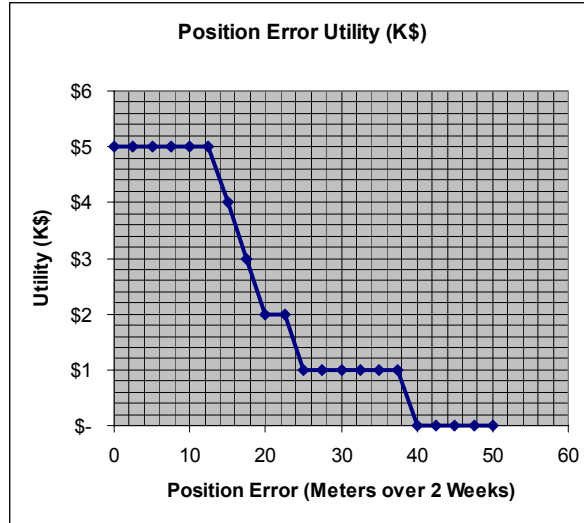


Figure 2.0-10 Position Error Utility

The Position Error Utility is extremely interesting, because it indicates an extremely high level of performance at a 12 meter error after 2 weeks as the most desirable performance and a useful range of less than 40 meter error as the worst allowable value. Meeting this level of performance could be extremely difficult, yet performance is ranked as the lowest value property for this sensor.

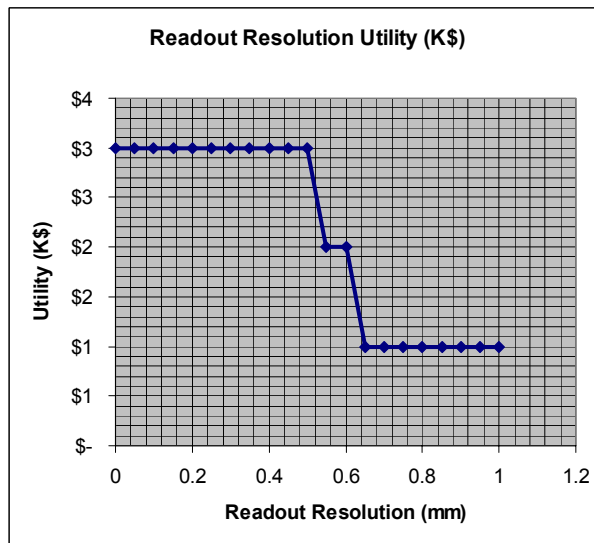


Figure 2.0-11 Readout Resolution Utility

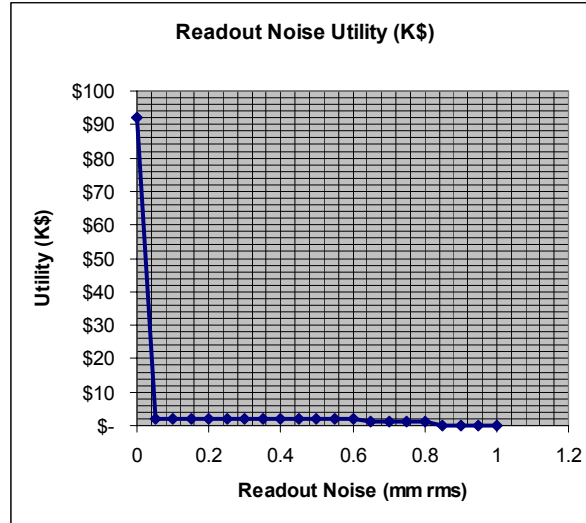


Figure 2.0-12 Readout Noise Utility

Error Mechanisms And Design Constraints

Error Mechanisms

A drag-free sensor proof mass, although shielded from the residual atmospheric drag and solar wind is still subject to a number of forces that can introduce erroneous accelerations. Table 3.1-1 below summarizes the known error mechanisms with critical parameter relationships and mitigation strategies. Error mitigation strategies that can be instituted by the host satellite operation/design in addition to the sensor design are indicated in italics.

Table 3.1-1 Drag Free Sensor Error Mechanisms

Error Mechanism Acting on Sensor Proof Mass	Typical Critical Parameter Relationships	Error Mitigation Strategy
Displacement of Proof Mass from Zero Self Gravity Point of Satellite	$(\text{Geometry Coefficient}) * (\text{Satellite mass}) * (\text{Proof mass displacement from satellite zero g point}) / (\text{Characteristic distance})^3$	<i>Select good geometry (geometry coefficient = 0 for hollow sphere). Maintain a small satellite mass. Provide large separation between proof mass and adjacent satellite mass. Limit displacement of proof mass from zero g point.</i>

Table 3.1-1 Drag Free Sensor Error Mechanisms (continued)

Error Mechanism Acting on Sensor Proof Mass	Typical Critical Parameter Relationships	Error Mitigation Strategy
Sensor Cavity Electric Field	$(\text{Electric field strength}) * (\text{Charge on proof mass}) / (\text{Mass of proof mass})$	<i>Shield electric fields.</i> Limit/discharge residual charge deposited from high energy particles and operational use. Decrease charge to mass ratio (dense proof mass).
Cavity Charge Image of Charged Proof Mass	$(\text{Charge})^2 * (\text{Displacement of proof mass from equilibrium point})^3 / \{ (\text{Characteristic distance to cavity wall})^5 * (\text{Mass of proof mass}) \}$	Limit/discharge residual charge deposited from high energy particles and operational use. <i>Limit displacement of proof mass from equilibrium point.</i> Provide large separation between proof mass and cavity walls. Decrease charge to mass ratio (dense proof mass).
Induced Magnetic Moment	$(\text{Magnetic susceptibility}) * (\text{Magnetic moment})^2 / \{ (\text{Characteristic distance to magnetic moment})^7 * (\text{Mass of proof mass}) \}$	Don't use ferromagnetic material for the proof mass! Use materials with low magnetic susceptibility for the proof mass. <i>Magnetically shield the sensor cavity.</i> Provide large separation between possible source of magnetic moments and the proof mass. Decrease magnetic force to mass ratio (dense proof mass with low susceptibility material).
Charged Proof Mass Motion Through Magnetic Field	$(\text{Charge on proof mass}) * (\text{Proof mass velocity}) * (\text{Magnetic field strength}) / (\text{Mass of proof mass})$	<i>Magnetically shield the sensor cavity.</i> Limit/discharge residual charge deposited from high energy particles and operational use. Decrease charge to mass ratio (denser proof mass). Orbital velocities cannot be reduced to minimize the interaction with Earth's magnetic field!

Table 3.1-1 Drag Free Sensor Error Mechanisms (continued)

Error Mechanism Acting on Sensor Proof Mass	Typical Critical Parameter Relationships	Error Mitigation Strategy
Capacitive Pick-off Displacement Force	$(\text{Pick-off area}) * (\text{Pick-off voltage})^2 * (\text{Proof mass displacement from equilibrium point}) / \{ (\text{Pick-off gap})^3 * (\text{Mass of proof mass}) \}$	Use optical pick-off technology! <i>Limit proof mass displacement from equilibrium point.</i> Decrease force to mass ratio (dense proof mass).
Photon Pressure from Optical Pick-off	$(\text{Pick-off light source power asymmetry falling on proof mass}) / (\text{Mass of proof mass})$	Balance illumination of proof mass. Limit power of pick-off. Decrease force to mass ratio (dense proof mass).
Residual Gas Brownian Motion Forces	$(\text{Gas density}) * (\text{Gas temperature}) * (\text{Proof mass area}) / (\text{Mass of proof mass})$	Minimize residual gas in sensor. Decrease area to mass ratio (dense proof mass).
Radiometer Force (Residual Gas Thermal Pressure Differential)	$(\text{Gas pressure}) * (\text{Gas temperature gradient}) * (\text{Proof mass area}) / \{ (\text{Gas temperature}) * (\text{Mass of proof mass}) \}$	Minimize cavity temperature gradients. Minimize residual gas and gas pressure in sensor. Decrease area to mass ratio (dense proof mass).

Design Constraints

After examining the error sources in Paragraph 3.1 above and considering other practical issues, the following design constraints/rules have been established for a drag free sensor:

High density proof mass –minimizes size or volume scaled error force to mass ratio produce smallest acceleration for given size.

Significant separation of proof mass from sensor case and adjacent satellite masses–minimizes effects of de-centered self gravity zero point. Can also permit satellite rotation if center of mass (rotation), and center of mass of the proof mass do not coincide.

Spherical proof mass – allows minimum clearance for full rotation of satellite or eliminates need for rotation control of satellite to proof mass.

Simultaneous three axis operation – this prevents any suspension forces constraining degrees of freedom from cross coupling into the sensitive axes of a limited degree of freedom sensor.

Magnetically insensitive proof mass – reduces need for complete magnetic shielding.

Conductive proof mass – prevents accumulation of embedded electric charge from high energy particle charge deposition that cannot be discharged.

Symmetrical readout illumination – helps minimize body fixed forces if satellite rotation not available for error cancellation.

Electric and magnetic shielding – prevents excitation of any residual charge

Thermal Gradient Control – minimizes effects of residual gas in cavity

Body Fixed Error Propagation vs Satellite Operating Mode

Notice: The perturbed form of the equations of orbital motion for small accelerations, the analytic techniques to integrate them over extended periods and the error impacts of various modulation schemes were obtained from effort funded by an internal Honeywell IR&D effort.

This material is considered Honeywell International proprietary and will be provided under separate cover.

Performance Verification

If a new sensor is developed for this application, some relatively inexpensive means of verifying performance of the prototype sensors short of orbital placement will be needed. Verifying the performance of any sensor with nano-g or better performance in a laboratory environment will be a significant challenge – perhaps much more so than the sensor development itself. This type of sensor application is unique in that the operating environment is actually the one in which errors can most easily be observed.

Design and Test Approach

In order to minimize the test costs and still provide confidence that the performance parameters can be met, the following design and test approach is recommended:

A. Design for Testability

Incorporate as many aids to verifying functional and performance capability into the sensor as possible. Understand the potential verification techniques before finalizing the sensor design.

B. Design for Robustness, Repeatability and Producibility

Keep the sensor design as insensitive to error sources as possible so that build variations do not change the response to error sources. Make the design easy to fabricate to tolerances and easy to assemble without adjustment so build variations are minimized. These guidelines will also help to keep the unit cost low.

C. Predict Performance through Analysis

Verify that the design meets all error budget requirements via analysis prior to testing. Understand the predicted performance in the test environment and the operational environment to supply appropriate test limits.

D. Verify Performance through Qualification Testing

Verify environmental sensitivities through ground qualification testing of one or two specially modified sensors and rely upon the design robustness and repeatability to ensure all units meet performance requirements.

E. Verify Function Through Acceptance Testing

Utilize short, inexpensive tests to determine that the sensor is meeting the functional requirements. Through qualification testing of a robust, repeatable design, this will ensure each shipped sensor will meet performance requirements without difficult, long, expensive testing.

F. Flight Test a Prototype Unit

Because of the expected relative low cost and size of a sensor developed to the requirements proved in this paper, it should be relatively easy (although not necessarily inexpensive) to piggyback a drag free subsystem on a space shuttle flight. This would obtain short term drag free performance while formation flying with the shuttle. For obvious cost and risk reasons, Honeywell does not recommend that the sensor control the shuttle in a drag free trajectory.

Qualification Test Approach

Although Honeywell does not feel that further exposition of any potential design and functional test approach is required for this paper, a technical approach to the qualification testing is outlined to illustrate that a ground test approach might be feasible. This approach was conceived and explored under Honeywell IR&D funding for exploring drag free flight technical problems.

This material is considered Honeywell International proprietary and will be provided under separate cover.

Sensor Design Solutions

Solutions depend on the level of integration with the satellite design.

A very simple sensor would provide:

- 1) A thermally controlled proof mass environment shielded from stray electric and magnetic fields with a magnetically inert proof mass
- 2) A mechanism to cage the proof mass during deployment and maneuvering
- 3) A proof mass position readout

This sensor would require satellite computations and control for error compensation, but can be fairly inexpensive to design and fabricate. An example concept is described in Paragraph 4.2.

A more advanced sensor/system could provide the capability to:

- 4) Actively communicate with the satellite processor (embedded sensor processor)
- 5) Self process/filter readouts and initiate thruster control
- 6) Generate a compensating force/acceleration to the proof mass based on trajectory analysis to cancel body fixed error sources without satellite rotation.
- 7) Perform periodic self-discharge of the proof mass by decoupling the thrusters to provide open loop drag compensation while temporarily activating the proof mass caging mechanism.
- 8) Adjust the sensor mounts to reposition the sensor so that the center of the proof mass coincides with the observed center of rotation of the satellite.
- 9) Utilize a gimbal system to isolate the sensor from satellite rotation
- 10) Utilize a cube proof mass with interferometer readout of position and angle to minimize displacement errors

An example sensor concept for the advanced case was beyond the scope of this feasibility study and would likely result in a sensor that is much more like the existing designs. Although Honeywell feels there are several approaches that could produce a more cost effective advanced design than those provided by the current technology, the multiple trade studies and error analysis to provide even a concept could not be covered by the existing project funding.

Impacts on satellite operation

Because satellite self gravity cannot be shielded, the design of the satellite, control of variable mass (fuel) and the placement of the sensor will be critical. Satellite rotation can average out the effects of self gravity, but add complications to the satellite operation and may expend additional fuel. It may also be possible to provide movable mass to compensate for fuel loss and/or misplacement of the zero self gravity point.

Simple Sensor

A simple sensor concept is illustrated in Figures 4.2-1 through 5. The sensor is based on a traditional accelerometer cylindrical form for ease of manufacturing. The sensor case is joined at the equator of the spherical proof mass cavity. This also facilitates manufacturing and testing. A spherical proof mass is constrained by a moveable cylindrical section that is retracted back into the case when the orbital trajectory has been achieved and the thruster system is capable of adjusting the satellite position to center the proof mass. The caging cylinder diameter was sized to ensure proof mass centering during activation. The case and proof mass are electrically conductive, non-magnetic materials. The case is magnetically and electrically shielded and would be designed with successive thermally insulating and conductive layers to remove external thermal gradients to prevent any radiometer errors. A simple optical readout system using

photodiode and LED arrays would be employed to provide symmetrical illumination and proof mass position detection. The symmetrical illumination will prevent photon pressure from producing any significant net proof mass acceleration. A set of optional add-on masses could be employed to make a completely spherical sensor and thereby remove any self gravity effects in the stand alone sensor.

The simple sensor design concept was sized to permit a moderate sized proof mass to minimize the error force/mass ration. Also, the design allows approximately .25" of proof mass clearance in the cavity. Although somewhat arbitrary, this amount of clearance should be within a manageable range of adjustment or calculation for the satellite center of mass/rotation should the host satellite undergo rotation. This will permit a slightly displaced satellite center of rotation to orbit the proof mass center of mass without bringing the sensor cavity walls into contact with the proof mass. If properly accommodated in the thruster control loop, this capability coupled with a spherical proof mass will allow rotational operation without continuous thruster firing to keep the center of rotation and proof mass center aligned. If the host satellite does not rotate and reduced performance is acceptable, a much smaller sensor less than ¼ the baseline size could easily be manufactured.

The only electronics in this sensor concept are solenoid force coils to latch and move the caging cylinder, LED intensity/constant current control, photodiode pre-amps and possibly a simple heater control to maintain the electronics temperatures or balance any case temperature gradients. Readout signal processing, thrust control and caging control is performed by the satellite processor.

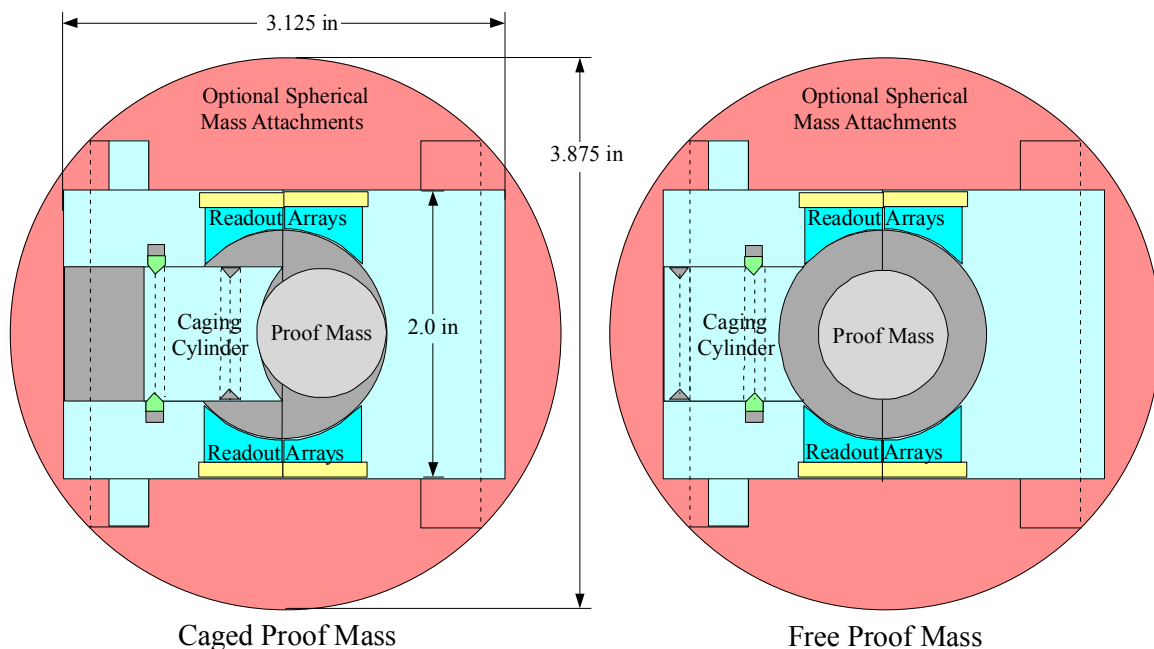


Figure 4.2-1 Simple Sensor Concept Cross Section

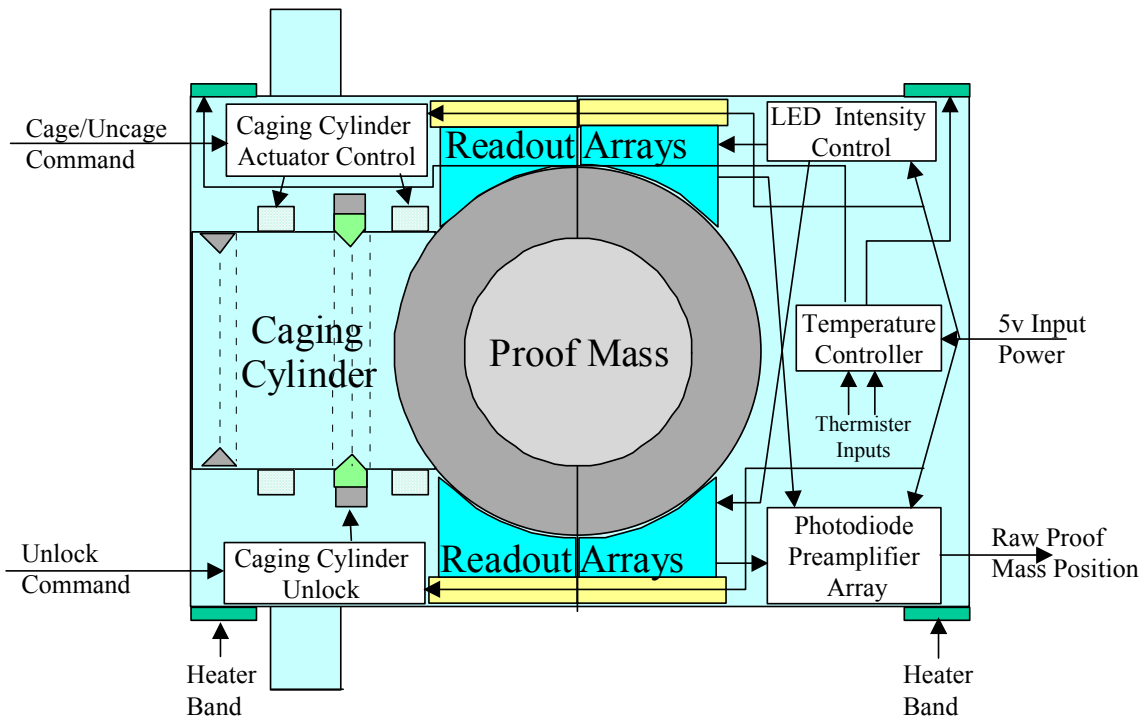


Figure 4.2-2 Simple Sensor Concept Functional Diagram

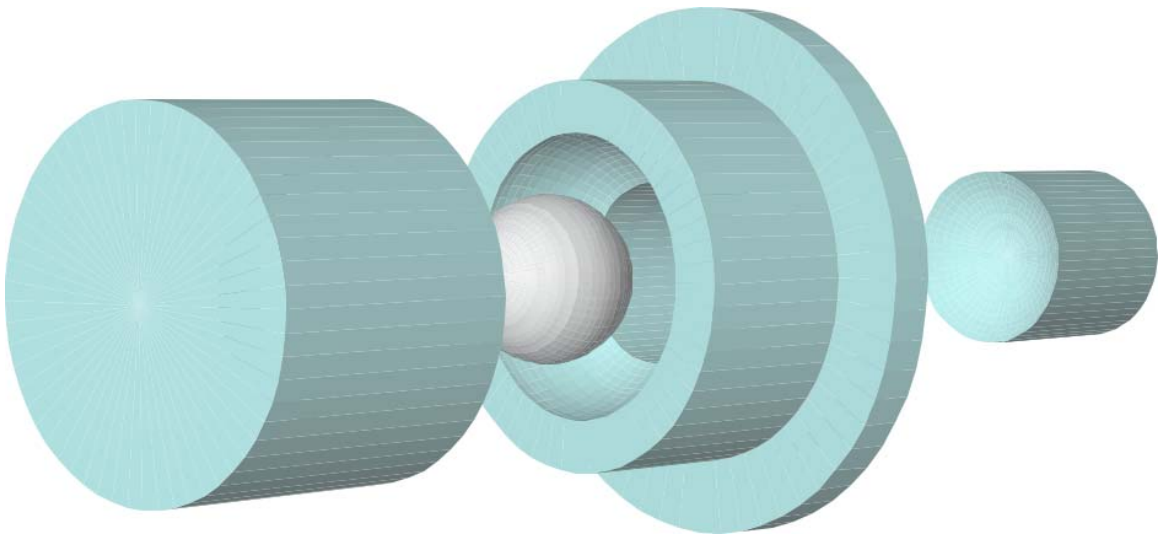


Figure 4.2-3 Exploded Bottom View

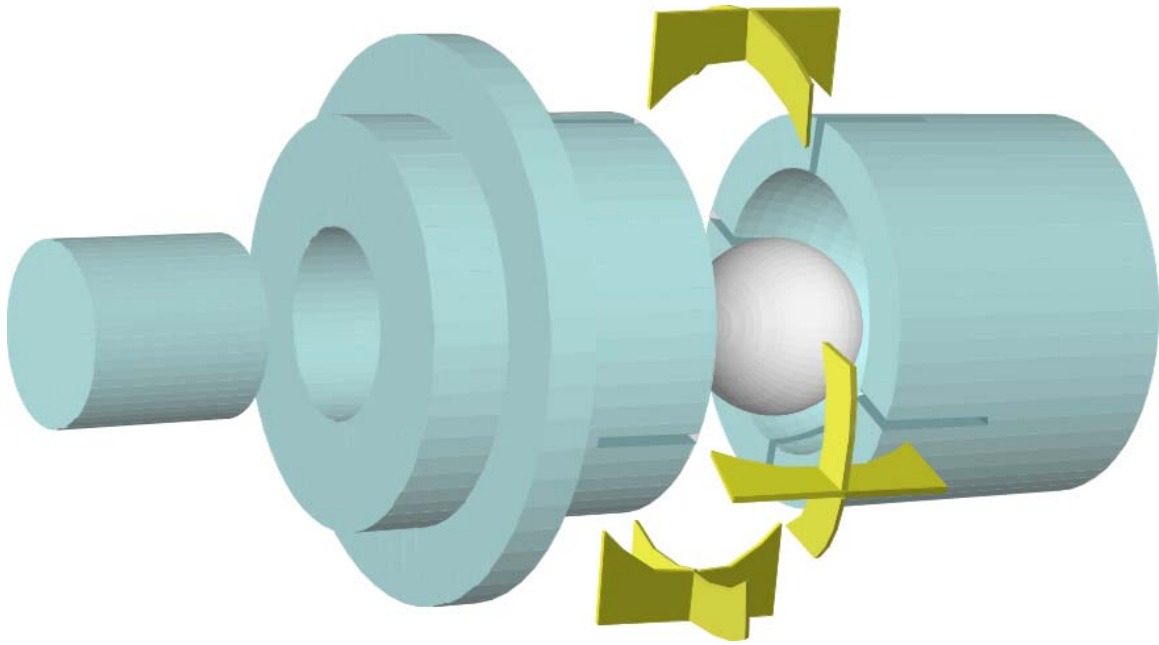


Figure 4.2-4 Exploded Top View Showing Optical Pick-off Arrays

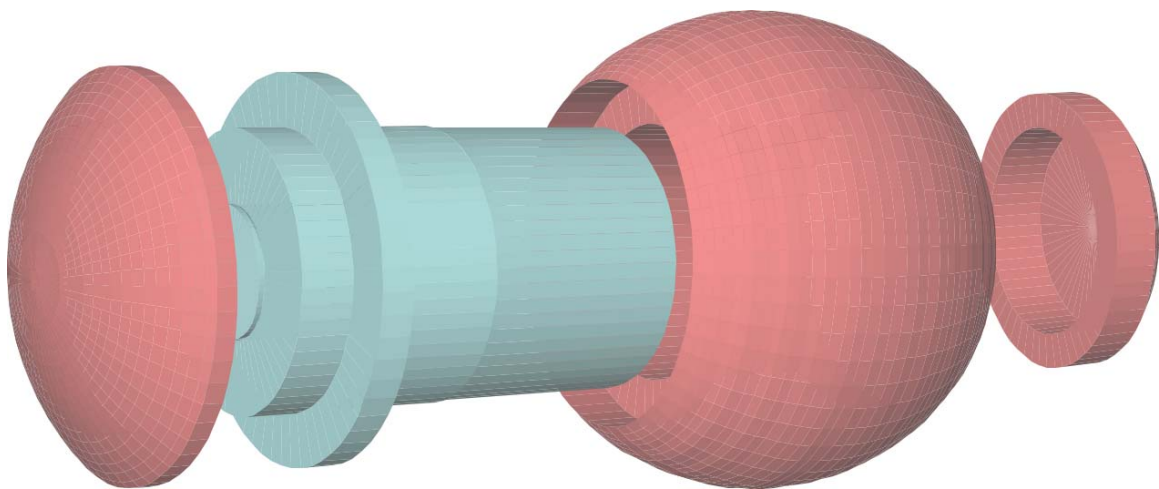


Figure 4.2-5 Exploded View Showing Optional Spherical Mass Elements

Table 4.2-I below show estimated property ranges and the resulting utility ranges for the simple sensor concept. Since this is only a concept there is a lot of uncertainty in the ranges of the properties. Nonetheless, it will allow a comparison to the more complex sensor concept presented below in Paragraph 4.3. The rationale for the unit price ranges are discussed in Paragraph 6.

Table 4.2-1 Simple Sensor Concept Estimated Properties

Property	Simple Concept Range	Utility Range (K\$ NRE)
Unit Price	\$10,000 - \$30,000	\$2,500 - \$2,200
Life	15 - 10 yrs	\$1000 - \$800
Power	4 - 7 watts	\$480 - \$260
Weight	1-2 lbs (.455 - .91 kg)	\$460 - \$410
Size	2" diameter x 3.125" height (optional 3.875 dia sphere)	\$33+ 35 + 35 = \$103
Reliability	>.98 @ 10 years	\$50
Performance	10 ⁻¹¹ g to 10 ⁻⁹ g (220 to 22000 along track meters in 14 days without rotational modulation or 0.0015 to 0.15 meters with rotational modulation)	\$60 - \$0
Readout Resolution	.1 - .5 mm	\$3
	Total Utility Range	\$4,656 - \$3826

Applicable Honeywell Technology

Honeywell has produced a wide variety of inertial sensors. For purposes of this report, the ones of interest can be broken primarily into gyro and accelerometer technologies, although other Honeywell products may also have some applicable technologies. The various sensor types have been examined for direct and indirect applicability to a drag-free sensor. There are really no directly applicable technologies that could be readily converted to a drag-free sensor having the desired accuracy. There are numerous areas of expertise that could be used in the design and fabrication of a totally new sensor suitable for drag free use.

Honeywell's inertial sensor expertise is probably the most applicable and useful resource we have to offer. Hundreds of years of combined experience have made Honeywell inertial sensor designers, users and analysts capable of producing a sensor with a fully understood set of error mechanisms that will perform as advertised at a realistic cost.

Accelerometer Technologies:

A. Electrostatic force balance of floating sphere (development prototypes only)

Before this study matured, the electrostatic sensors appeared to have a lot of relevance to a drag free sensor. It turns out that they are not a good basis, however. The proof mass in both the gyro and accelerometer are hollow beryllium spheres with a very poor mass to size ratio so that a weak electrostatic suspension system can be used. The electrostatic suspension requires small cavity/proof mass clearances and may leave the proof mass with a net charge after lift-off. The spheres are also

expensive to produce, are made of a hazardous material (beryllium) and the technology has been discontinued in favor of optical gyro technology. The accelerometer design is essentially the same as the electrostatic gyro mechanical element illustrated under **E** in the Gyro Technologies. The beryllium rotor would not be etched for spin optical axis determination and the spin motors would not be present. Acceleration is determined from the electrostatic force required to null the sphere position in the capacitance position sensors. Development of this sensor never proceeded beyond prototype evaluation. Simulated low g testing was attempted by floating the sensing sphere in pressure density controlled sulfur hexafluoride to null most of the laboratory 1 g field! Historical information on this sensor is rare so there is an additional relearning risk if this technology was applied. However, there are a few engineers still employed with some knowledge of this sensor.

B. Electromagnetic force balance pendulum



Figure 5.0-1 QA-3000

This technology has been the mainstay of the Honeywell QA series accelerometer line. The pendulum position sensing is capacitance based and a rebalance current is applied to pendulum torque coils to null the sensor. The sensor is small and relatively inexpensive to produce, depending on the desired accuracy. Some fabrication techniques might be applicable and the electrostatic sensing mechanism could also be applied. The sensor noise floor is around 1 micro-g and cannot be lowered without a major redesign, although some range shift can improve low g capability. Thermal noise in the pendulum hinge will eventually prove to be a limiting factor.

C. Gyroscopic torque balance of pendulum



Figure 5.0-2 Specific Force Integrating Receiver (SFIR)

This technology has proved to be the lowest noise and highest accuracy method of sensing acceleration. It is also the highest cost production accelerometer ever made by Honeywell. An unbalanced, floated spinning mass gyro is held at an output axis null by a forced precession of the gyro assembly. The output rotation angles are obtained from an inductive angle sensor. The precession angle of the gyro assembly is sensed by a dual speed resolver and provides a direct velocity readout. Acceleration measurements needed during calibration are obtained by numerical differentiation of the output. The sensor noise floor is below .1 micro-g, but again, further improvements would be extremely expensive. This sensor is no longer in production at Honeywell, although refurbishment of existing sensors is performed. Most of the materials and processes used in this sensor would not be considered producible in today's production environment. Due to the nature of the readout mechanism, at very low input levels the quantized velocity output frequency becomes so low that any attempt to filter the output noise becomes useless. Some of the precision fabrication techniques might be useful in some drag free sensor designs.

D. Open loop vibrating beam



Figure 5.0-3 Accelrex Quartz Vibrating Beam Accelerometer (VBA)

This sensor employs a conventional pendulous mass to but restrains its motion in an open loop fashion with two vibrating beams. The detected difference frequency of the differentially stressed vibrating beams provides the output signal. This technology is intrinsically highly producible and can achieve sub micro-g noise levels. Prototype instruments have been used as absolute gravimeters in oil drilling applications. Although used in tactical grade accelerometers, this technology for high precision applications has not been pursued after being abandoned by the strategic weapons community. Like virtually all of the traditional inertial sensors, there is no laboratory test data at extremely low g levels and there may be unknown dead zones or extreme non-linearities in the region between 1 and .001 micro-g's

Gyro Technologies:

E. Electrostatically suspended rotating sphere with optical readout

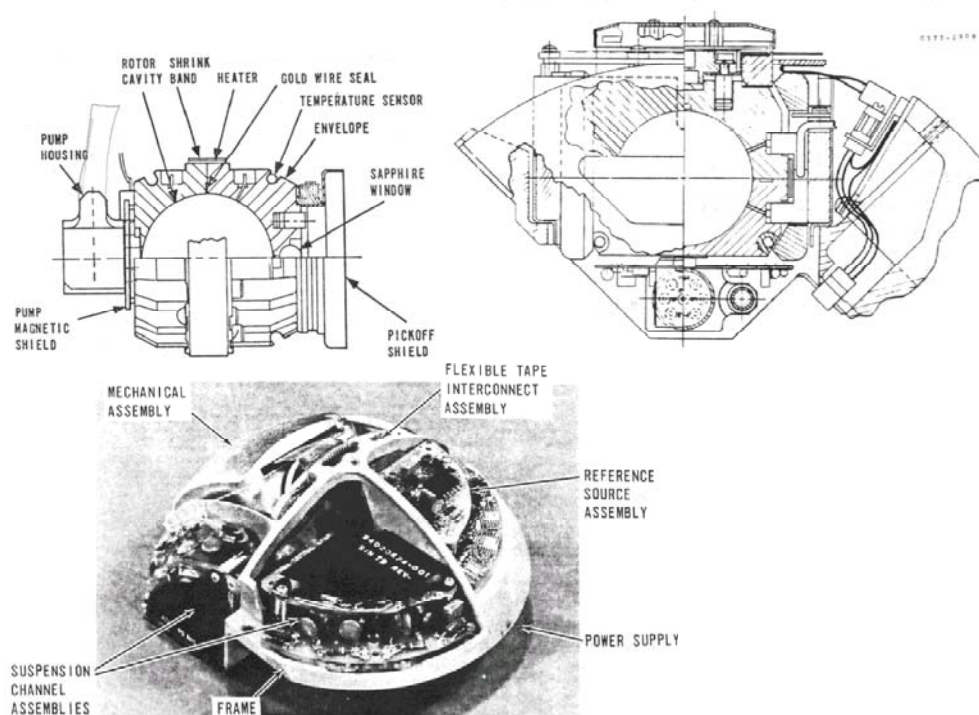


Figure 5.0-4 Elements of the Electrostatic Gyro (ESG)

This instrument electrostatically suspends a hollow spinning beryllium sphere. The spin axis is detected by optical means observing etched patterns on the sphere. The spin axis location is used as a non rotating inertial reference. The mechanization produces a very low noise, high precision instrument for detecting rotation. An earlier (1974) attempt has been made to convert this gyro technology to a low g accelerometer as discussed in A above. The machining technology to produce very high tolerance spherical cavities (and spheres) might be applied to a drag free sensor. Certainly the electrostatic suspension system, although based on outdated technology could be adapted to current technology and serve as a suspension system of force correcting system in a drag free sensor if desired.

F. Conventional spinning mass



Figure 5.0-5 Third Generation Gyroscope (TGG)

As a strategic weapons sensor, accuracy was paramount in the design of this sensor at the expense of cost and producibility. This is a classical single degree of freedom integrating gyroscope. A balanced, spinning mass gyro is floated at neutral buoyancy in a damping fluid. Rotations around the input axis are converted through the damping and the gyro dynamics to rotations about the output axis. This rotation is sensed by inductive resolvers and used to control gimbals to maintain the output at null. This offsets any input rotations and keeps the gyro stationary in inertial space. The potential technology that might be useful is the advanced thermal control mechanisms used to eliminate gradients. The outer case is multiple layers of conductive and insulating material that disperses external gradients and heater induced gradients uniformly around the gyro element.

G. Ring laser gyro (RLG) - resonant cavity interferometer



Figure 5.0-6 GG1320 Radiation Hard Gyro

Although not an “inertial” sensor in the traditional sense, because no inertial properties of mass are involved, the ring laser gyro detects rotation through the frequency change introduced to two coherent counter rotating light beams that see a different path length/cavity length when the gyro is rotated. The natural HeNe laser frequency in each path shifts to maintain integer wavelengths in the effective cavity length. The spatial beat frequency (interference fringes) of the combined beams is

detected to provide a measure of rotation. Mechanical dither about the input axis is provided to prevent the two beams from locking in frequency at very low rotation rates. This sensor is very mature and has a very low unit cost when built for aircraft applications. Unfortunately, because no mass effects are involved there is no direct applicability to a drag free sensor. Indirect application of the laser technology, however could be applied in numerous ways such as: Production of an interferometer readout of a proof mass position for flat, mirrored proof masses. The Zerodur optical material machining technology would permit very cost effective machining of any transparent, low coefficient of thermal expansion sensor material. The getter technology used to promote long laser life could also be applied to the removal of residual or outgassed gas molecules in a sealed drag free sensor. The optical detection technology might also be useful for generic optical readout mechanizations. Finally, the piezo-electric technology used to control the optical path length could be used as an actuator mechanism for a small gap caging mechanism.

H. Fiber optic interferometer

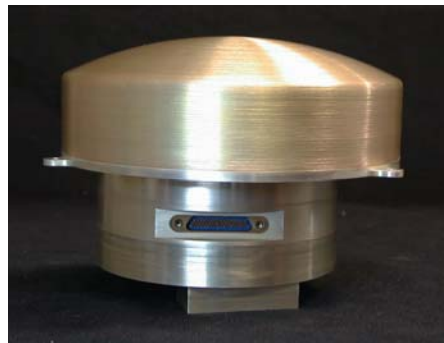


Figure 5.0-7 Honeywell Precision Navigation Fiber Optic Gyro

Again, this is not an “inertial” sensor in the strict sense. Like an RLG, it detects rotation through the interference of two counter rotating light beams traveling through a fiber optic coil. However the beam frequency is not dependent on an effective resonant cavity length, only on the virtual path length differences caused by the rotation. Consequently, the path length has to be very large to see the small frequency difference. The high precision instruments that Honeywell produces null the beam phase differences through an opto-electric modulator and the drive signal is used as the readout, while the optical signal is merely used to null the opposing beams’ phase differences. The possible indirect applications to a drag free sensor are the solid state laser technology and the photo-detector technology.

Other Technologies:

I. Reaction Wheel Assemblies



- **0.028 Nm Torque**
- **1 Nms Angular Momentum**
- **1.3 Kg Weight**
- **<6W Power**

Figure 5.0-8 HR04 Miniature Reaction Wheel

Honeywell produces a wide range of reaction wheels suitable for attitude control on satellites of all sizes. The most recent product entry for small satellites is shown above. Since reduced size and weight were criteria for a drag free sensor, Honeywell has assumed that a smaller size satellite would be considered for missions utilizing the sensor. A reaction wheel would be necessary to achieve the error canceling satellite rotations discussed in Paragraph 1.1.4 earlier. The use of solar power and reaction wheels rather than attitude thrusters to maintain the rotations would allow assignment of all thruster fuel to maintenance of a zero drag trajectory.

J. Bus Controllers

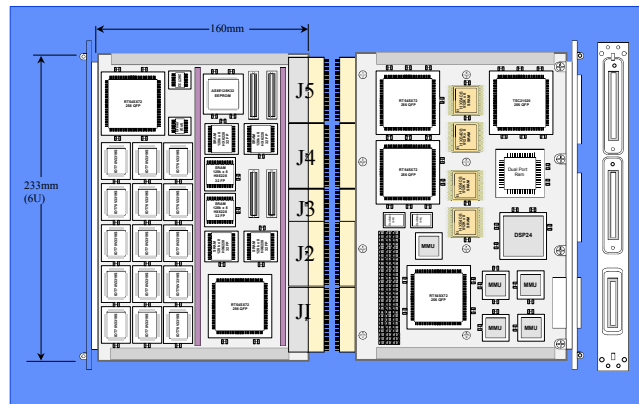


- RHPPC 35-210 MIPS
- 6Ux220, 3.5 lbs., 14W (nom)
- IEEE1394 backplane
- MIL-STD-1553
- UART
- High Speed Serial
- CCSDS telecommand port
- CCSDS Telemetry
- Fault Management
- On-board Power Supply

Figure 5.0-9 RHPPC Spacecraft Bus Controller

Again, assuming size is critical, Honeywell has developed a single card Power PC based bus controller to integrate satellite subsystems.

K. Processors



- RT21020/RHDSP24
- 2-3 GFLOPS sustained
- 6Ux220, 2.2 lbs., 16W (nom)
- cPCI backplane

Figure 5.0-10 Radiation Hard Vector Processor

Along with the Power PC based products, Honeywell is also developing a single board vector processor for high capacity on-board satellite data processing. A processor with this high capacity could potentially serve the entire satellite and perform the computations necessary to compensate and manage even a very complex zero-drag system along with the other on board sensors and systems.

L. Micro-Thrusters

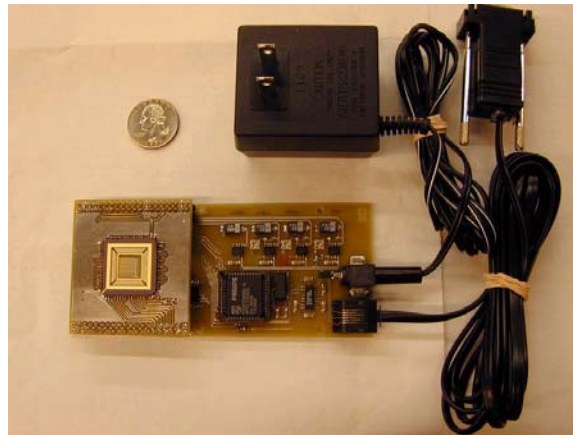


Figure 5.0-11 Honeywell – Princeton MEMS Megapixel Micro-Thruster Development Unit

Although not yet producing these as a product line, Honeywell has teamed with Princeton University to explore the development of “digital” micro-thrusters. In the full size envisioned by the designers, this type of micro-thruster would contain up to 250000 “pixels” for drag canceling thrust generation. In the prototype versions, they are not practical for long duration missions, but they certainly represent a potential path to a very lightweight, reliable thrust system. Honeywell’s involvement in this type of research brings a full spectrum of experience to potential drag-free applications.

Capabilities Summary

Table 5.1-1 Honeywell Applicable Technologies and Capabilities Summary

Sensor Type	Direct Drag Free Applications	Indirect Drag Free Applications
A. Electrostatic Accelerometer		
B. Pendulous Accelerometer		High volume, low cost sensor fabrication. Electrostatic sensing.
C. Pendulous Gyroscopic Accelerometer		Precision fabrication/testing techniques

Table 5.1-1 Honeywell Applicable Technologies and Capabilities Summary

Sensor Type	Direct Drag Free Applications	Indirect Drag Free Applications
D. Vibrating Beam Accelerometer		
E. Electrostatic Gyroscope	(discontinued product)	Spherical cavities and sphere machining techniques. Electrostatic suspension system.
F. Single Degree of Freedom Spinning Mass Gyroscope	(discontinued product)	Thermal control mechanisms
G. Ring Laser Gyroscope	Low cost medium precision satellite attitude sensing.	Interferometric position readout. Optical material machining, getter, photodetector, piezo-electric actuator technologies
H. Fiber Optic Gyroscope	Long life, low noise, high precision satellite attitude sensing	Solid state laser and photodetector technologies.
I. Other – Reaction Wheels	Satellite attitude control	
J. Other – Bus Controllers	Integrated satellite communications systems	
K. Other – Processors	High throughput, space environment data processing	
L. Other – Micro-thrusters	Drag canceling thrust generation. Development experience with micro-thrust community.	
All	Space and missile sensor/systems design, error modeling expertise.	

Sensor Cost Range Estimates

Due to the preliminary nature of the sensor concepts and the lack of firm requirements, the following discussion should not be interpreted as a ROM or any other type of quote to design, build or supply a drag free sensor. The cost ranges of available Honeywell products are discussed and compared to the expected complexity of sensor similar to those described in Paragraph 4.

Honeywell will be pleased to provide an approved ROM or other quote upon formal request from NASA.

Simple Sensor

Simple Sensor Recurring Cost

The simple sensor without a processor is not significantly different in construction complexity than the Honeywell QA series of accelerometers. These accelerometers are priced primarily by the yield at a specific performance level, the amount of testing required to verify specified performance and the quantity purchased. Prices range from <\$1,000 to \$50,000. Since this sensor has very little tight tolerance machining or extensive acceptance testing and no screening with an assumed 100% yield a price range of \$10,000 to \$30,000 for small quantities would be expected. This price range assumes that minimum lot parts buys are included in non-recurring costs. Otherwise, minimum parts buys for a single sensor could run the cost up substantially if the design does not use standard parts stocked by Honeywell. Experience has shown that this could extend the range to \$250,000. If quantities of several hundred or more were ordered, the unit price range would drop to \$5,000 to \$20,000. More accurate estimates could not reasonably be made until a more mature design concept and firm requirements are available.

Simple Sensor Non-Recurring Cost

This cost is driven by the documentation and quality processes demanded by the customer as well as the design and verification difficulty. For a product with a large potential market and significant return on investment, Honeywell could offset some or all development costs. Without considering the development of a suitable ground or flight test verification program, development costs for existing system products have run from \$5M to \$25M. Since this is a single sensor, it is likely to fall on the low end of this range, however the technical risk component is significant since a similar product has never been successfully produced (excluding the electrostatic accelerometer development effort in the early 1970's). The unproven market and potential risk would likely constrain Honeywell to only accept a cost plus development contract.

The cost to develop and conduct a performance verification program could be significant. Although possibly more cost effective than on-orbit flight testing, the testing scheme described in Paragraph 3.4.2 could be a significant fraction of the sensor development costs. Although Honeywell has no prior experience in the development of the specific test, all of the electrical and mechanical components, save the torsion element of the pendulum have been used or built for previous inertial test apparatus. Assuming a dedicated rate table or extensive facility modifications were not required, the cost might range from \$500K to \$2M. This would include extensive error analysis and test software development.

Complex Sensor/System

Complex Sensor Recurring Cost

Without a concrete concept, a reasonable cost estimate cannot be made, but upper range values can be estimated from existing systems. A complete Attitude Reference Unit for moderate accuracy space applications with a processor, power supply and three ring laser gyroscopes can be purchased for under \$200,000. Very high performance Attitude Reference Units with sensor and processor redundancy can cost up to 10 times more. The SFIR, which was one of the most expensive single sensor devices made by Honeywell could be purchased for less than \$200,000. Based on these and other products, a complex sensor with a space qualified processor and significant mechanical complexity with tight tolerances could likely run from \$50,000 to \$250,000 but in no case reach exceed \$1,000,000 unless currently unknown requirements were presented.

Complex Sensor Non-Recurring Cost

Due to the potential complexity and implied additional accuracy required for this sensor, the development costs would probably reach the high end of the \$5M to \$25M range. Test development costs due to the added accuracy and possible inclusion of additional system elements such as micro-thrusters could double the performance verification development costs.

Summary

This study effort along with a Honeywell funded IR&D project has yielded a simple sensor concept, a satellite operation methodology (Paragraph 3.3) for achieving desired station keeping accuracy with a moderate accuracy sensor as well as a unique ground test method (Paragraph 3.4.2) for verifying performance. The recurring cost range for the simple sensor is well below the current cost of existing sensors, with moderate development costs. Clearly, the development of such a sensor is feasible – particularly with a potential ground test method to verify design approaches and error source magnitudes.

Honeywell would be pleased to pursue further drag free sensor and test method development on future contracts. Potential areas that would be fruitful in maturing concepts and costs would be:

- A. Development of integrated satellite/sensor operational scenarios
- B. Proof-of-principle development of torsion pendulum test approach. Perhaps leading to the Honeywell capability to become a centralized verification agency for all zero-drag ground performance verification. Honeywell excess precision inertial sensor test facilities could be put to good use in this scenario.
- C. Refinement of sensor requirements – perhaps based on mission need scenarios
- D. Proof-of-principle demonstration of some or all of the simple sensor design concepts such as the photodiode readout array and caging mechanism.
- E. Further exploration of the potential complex/high accuracy sensor/system configurations.

Supporting Data